Title: **Ink Material Selection and Optical Design Considerations in DLP 3D Printing**

Authors: **Hossein G. Hosseinabadi [a], Daniel Nieto [b,c], Ali Yousefinejad [a], Hoda Fattel [c], Leonid Ionov [a,*], Amir K. Miri [c,*]**

Affiliations:

[a] Faculty of Engineering Sciences, Department of Biofabrication, University of Bayreuth, Ludwig Thoma Str. 36A, 95447 Bayreuth, Germany

[b] Complex Tissue Regeneration Department, MERLN Institute for Technology Inspired Regenerative Medicine, Universiteitssingel 40, 6229ER Maastricht, The Netherlands

[c] Department of Biomedical Engineering, New Jersey Institute of Technology, 323 Dr Martin Luther King Jr Blvd, Newark, NJ 07102, USA

[*] Co-corresponding Authors:
Dr. Leonid Ionov, Faculty of Engineering Sciences, Department of Biofabrication, University of Bayreuth, Ludwig Thoma Str. 36A, 95447 Bayreuth, Germany (leonid.ionov@uni-bayreuth.de)
Dr. Amir K. Miri, Department of Biomedical Engineering, New Jersey Institute of Technology(am3296@njit.edu)

Email Addresses of Authors:
H.G.H. (Hossein.goodarzi-Hosseinabadi@uni-bayreuth.de), D.N. (daniel.nieto@usc.es), A.Y. (Ali.Yousefinejad@uni-bayreuth.de), H.F. (hf82@njit.edu), L.I. (leonid.ionov@uni-bayreuth.de), A.K.M (am3296@njit.edu)

1. Contents

Abstract

Digital light processing (DLP) 3D printing has become a powerful manufacturing tool for fast fabrication of complex functional structures. The rapid progress in DLP printing has been linked to research on optical design factors and ink selection. This *critical review* highlights the main challenges in DLP printing of photopolymerizable inks. The kinetics equations of photopolymerization reaction in a DLP printer are solved, and the dependence of curing depth on the process optical parameters and ink chemical properties are explained. Developments in DLP platform design and ink selection are summarized, and the role of monomer structure and molecular weight on DLP printing resolution are shown by experimental data. A detail guideline is presented to help engineers and scientists to select inks and optical parameters for fabricating functional structures toward multi-material and 4D printing applications.

Keywords: Digital light processing, 3D printing; photosensitive monomer; ink selection; resolution improvement.

1. Introduction

Digital light processing (DLP) printing is a layer-wise two-dimensional (2D) crosslinking of photosensitive inks per light exposure. DLP printing has found extensive applications in the rapid prototyping [1], tissue engineering [2,3], and regenerative medicine [4]. The market value was around US $370M in 2020, with an anticipated 25% compound annual growth rate between 2022 and 2026 [5]. The main applications today include fabrication of medical devices and healthcare equipment [6], surgical guides for dentistry, wax models for jewelry, sculptures for the aesthetics industry, and metamaterials for the soft robotics [7,8]. There is an increasing tone to use DLP printing for tissue engineering applications. Many endocrine diseases such as diabetes represent failure in an organ system. Organ failure or loss of organ function is becoming the number one cause of death worldwide [9]. Since organ shortage is an impending health care crisis, DLP printing of the tissue or organ blocks is becoming a promising therapeutic option. Only diabetes affect ever growing four hundreds of millions of people [9]. Biofabrication and transplantation of islets of Langerhans is considered as an effective therapeutic procedure that enables insulin independence for diabetic patients [10,11]. However, rapid fabrication of fully vascularized tissues and living organs with current technologies is not yet achieved. Despite tremendous advancements [12], the research field is stalled at fabrication of layers of live tissue that lack adequate variety of hollow constructs and capillaries compared to the microenvironment of a natural tissue. In this ground, DLP overcomes the current challenges in fast fabrication of tissue building blocks at a high fidelity [2] to target a long-lasting challenge to make three-dimensional (3D) tissue scaffolds at a clinically relevant time scale [13]. The rate of DLP printing is much higher than conventional additive manufacturing methods such as extrusion 3D printing [14,15].. In extrusion 3D printing the shear forces can damage the cell membrane and reduce cell survival.

DLP printing occurs through light projection with two work principles. Liquid crystal displays (LCDs) and digital micromirror devices (DMDs) are used to direct the light as squared voxel patterns onto an ink material [4,16]. Examples of simple LCD- and DMD-based projectors are shown in **Figure 1a** and **Figure 1b**, respectively. The LCD works by transmissive planar light patterns, while DMD works by reflective processing of digital patterns. The LCD projectors have found fewer applications in 3D printing because of their inability to transmit high intensity and high energy (UV) lights through the liquid crystal material [4,17,18]. As an alternative to LCD projectors, most recent endeavors in the research field are focused on the exploitation of a DMD chip [19]. DMD is a micro-electromechanical semiconductor device designed to reflect a patterned high-intensity UV light from a light emitting diode (LED) source onto a photocrosslinkable hydrogel system to print high-fidelity structures [20].

In general, 3D printing technologies can be classified into contact-based and contactless methods. The common contact-based methods consist of fused deposition modeling (FDM), extrusion, and inkjet printing. FDM is an affordable method of 3D printing based on extruding a thermoplastic polymer around melt temperature. Extrusion 3D printing has the versatility and affordability in making small to large structures [16]. It is a low-cost technology that benefits from a relatively high fabrication speed [21] and the control over the mechanical properties [22]. However, extrusion 3D printing has much worse resolutions, ca. 100-1200 µm, compared to inkjet 3D printing, ca. 10-50 µm [23]. Inkjet 3D printers deposit liquid-binding inks, benefiting from multiple reservoirs to be used for multi material direct writing [21]. The low speed and high shear forces [24], along with the possibility of needle clogging, limits the use of this technology. Contactless methods consist of fabrication by stereo-lithography (SLA) and digital light processing (DLP) 3D printing [25,26]. SLA is a solid freeform additive manufacturing [27,28], which uses the light in LASER form to sweep the ink surface for crosslinking and fabricating structures. It has a practical resolution of 40-150 µm [29]. DLP benefits from a much higher speed [30], an easy control over the mechanical properties [22], and a superior scalable resolution down to 1 µm compared to other methods [18]. The speed of fabrication is typically as high as 0.5 and 15 mm/s [18,31]. While being established for rapid prototyping of polymeric structures, DLP printing has enabled creation of tissue-like structures with microstructures and stiffness values similar to those of biological tissues [7]. The blood vessels shown in **Figure 1c** represent the *in vivo*-like architectures in a real heart organ. Compared to other 3D printing techniques, DLP printing is among the most promising technologies that may enable us to fabricate such a complex organ with vessels ranging from 5-20 µm (capillaries) to 2-3 cm (aorta) at a clinically relevant resolution and speed. **Figure 1d-i** shows a DLP printed example of veins with multiple sizes using poly-ethylene glycol diacrylate (PEGDA) ink. When adding other components to pure photosensitive monomers, we expect to have light scattering issues. **Figure 1d-ii, iii** shows that adding 1% w/v glass microbeads, which mimics light scattering in the presence of any agents in the bioink (i.e., ink with cellular capacity), leads to the clogging of the 3D printed vessels and failure of the vessel to transport fluids. The clogging practically blocks the transfer of oxygen and nutrients by the DLP printed construct. This concern shows the need for further investigations into the material selection, and a better understanding of light-material interactions such as refraction, scattering, and absorption kinetics in DLP platforms.

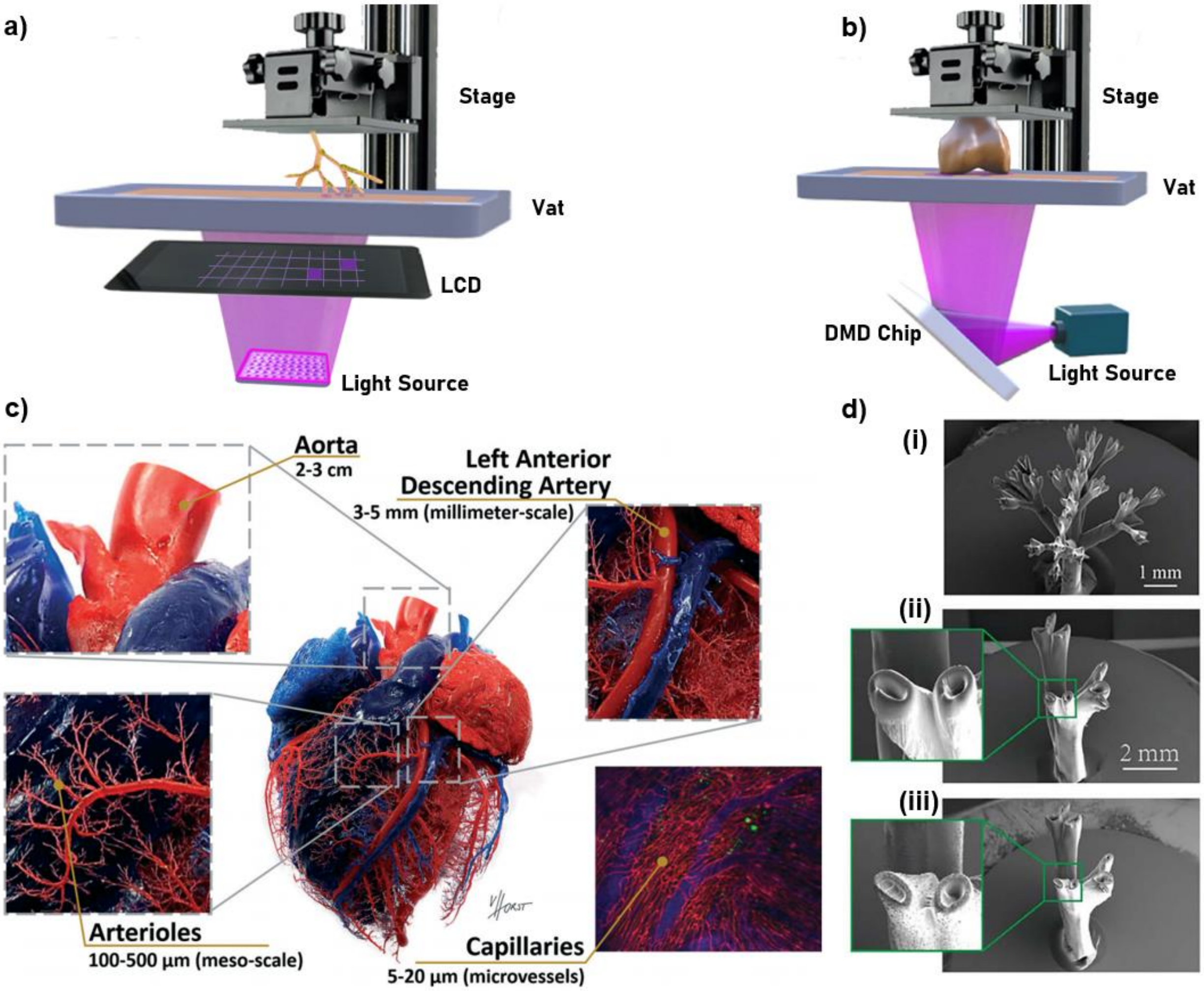

Figure 1. DLP 3D printing, **a)** a typical LCD-based platform as a transmissive method for 2D patterning of the light, **b)** a typical DMD-based DLP platform as a reflective technology for 2D patterning of the light, **c)** An anatomical photograph of a porcine heart showing the diversity in a natural biological organ (red represents the arterial blood supply and blue represents the venous blood supply) obtained by corrosion casting [32], **d)** a successful production of an **(i)** fractal tree, **(ii)** a hollow blood vessel with a pure non-scattering material (PEGDA, 1% w/v Irgacure 819), and zoom-in detail of vessel opening, **(iii)** the same material including light scattering bead (glass beads of 4 µm diameter, 1% w/v) resembling scattering due to presence of live cells, leading to the formation of clogged blood vessels through DMD-DLP printing [33].

DLP printing is shifting the manufacturing paradigm by cutting down the build time. In contrast to the conventional stereolithography (SLA), a DLP do not cure the ink with sweeping a guided laser but with a projection of an entire layer at once. This digital projection necessitates different mechanisms for light-material interaction which are rarely discussed in the literature. A deeper insight into molecular structure of photopolymerizable inks and the kinetics of photopolymerization reaction is required to harness the capacity of DLP printing for achieving high spatial resolutions and defined architectures toward applications such as tissue and organ regeneration. A better understanding about governing equations helps to reach high fabrication speeds to fulfill the growing demand for mass production..

To address these shortages, the core of this review is placed on ink selection and designs in DLP printing. This *review* starts with summarizing significant technological advancements in improving DLP printing platforms. The role of the ink chemistry and the monomer molecular structure in enhancing the performance of DLP platforms are then explained. The kinetics equations of light absorption and photopolymerization reaction in DLP printers are described, and their applications to control the curing depth based on the processing parameters such as the light intensity and the exposure time are illustrated. The discussions help material scientists and bioengineers select proper materials/inks and understand fundamental design considerations for improving 3D printing resolution when using a DLP platform. Other light-patterning technologies such as point-by-point light patterning in laser-induced forward transfer method [34], layer-by-layer light patterning in LCD-based stereolithography, or volumetric light patterning in multiphoton polymerization methods [35,36] are not discussed here as a focus to keep the integrity of review, however their concepts are almost similar to DLP. In post-processing, combined photopolymerization reaction kinetics and Euler-Bernoulli beam theory can be implemented to study post-curing induced shape distortion of thin structures prepared by DLP [37]. Mechanical behavior of printed samples during post-printing process is correlated with printing parameters (such as light exposure time used for each layer, height of each layer, and light intensity), post-curing light intensity, and thickness of the structure. Details of various methods for improving the quality of printed structures by post printing approaches are discussed elsewhere [38].

2. Applications and Limitations of DLP printing

Here, we briefly summarize the applications and limitations of DLP printing which are extensively discussed in previous review papers [4,39]. DLP fabrication speed can reach as high as 1000 mm^3/s in a volumetric scale [40] and show enhanced resolutions as precise as 1-10 µm. It is among the best achievable fabrication speeds and resolutions in 3D printing industry. It makes DLP a proper candidate for microtissue applications [4]. Fast creation of complex structures with micrometer-sized resolutions allows fabrication of micro-vascularized tissue models to be used as vasculature or disease models. Two major applications of these models are tissue fabrication for clinical transplantation, and fabrication of tissue-engineered models to investigate disease pathologies, and pharmaceutical compound screening [41]. DLP can be used for drug discovery, drug delivery, and screening in micro-tissue models of lung [42], liver [43], bone [44], heart [45,46], spinal cord [47].

Due to the high speed of DLP printing, physicians can rapidly prepare 3D models of a patient pathological organ. In the clinical treatment of a variety of acute diseases, such as myocardial infarction, cerebral hemorrhage, and cerebral infarction the effective treatment window is only a few hours, requiring the surgeons to prepare the patient surgical plan within a few minutes. Compared to other methods, using DLP one can program a series of processing parameters such as exposure time, light intensity, and light wavelength to build a 3D structure with a relatively high accuracy and adjustable physio-mechanical properties [7]. DLP printed disease models are also useful for the teaching of clinical medicine, especially the basic subjects of medical education such as anatomy. DLP can quickly print personalized dental teaching models of sufficient dimensional accuracy so the students can get an intuitive impression of oral malformation diseases [48]. Medical devices such as implants can be printed with DLP printers using biodegradable [49] or non-degradable [50] materials towards in vivo applications. Implants are used to replace or repair the injuries in vivo. DLP is capable of building implants to match with the injured part and then guide the tissue regeneration at the interface. A fundamental challenge in producing tissues for clinical use lays on the difficulty in producing functional vasculatures with biocompatible materials. The diffusion limit of nutrient and waste transport in tissues is limited to around 250 µm. Larger tissue constructs critically need vascularization to maintain cell viability in clinical practices [40]. DLP printing is in theory capable of producing highly vascularized constructs. However, there exist a few ink materials which provide the required resolution and at the same time provide the favorable biocompatibility and bioactivity for tissue regeneration. Conventional SLA and DLP printing require large volumes of photo-polymerizable inks which increases the production costs. Another limitation is the need for costly equipment, especially for particular optical designs. In next section, we review different DLP strategies and their optical designs.

3. Design Models of DLP Platforms

3.1. Different DLP Printing Strategies

Depending on the ink formulation, different types of light projectors can be integrated into the design of a DLP platform ranging from infrared [51] to ultraviolet light [2]. Wang et al. [52] developed one of the most straightforward designs, using a commercial white light projector (~ 2500 lumen at visible wavelength range) for light patterning and crosslinking a hydrogel layer with a low speed of around two minutes per layer. Commercial light projectors generate vast amounts of energy which can heat the polymer vat to above 40ºC in ~ 15 minutes [52]. More advanced DLP platforms use more optimal light sources besides optical considerations.

Many advancements in optics design are devoted to improving DLP capabilities to print implantable microtissue models. This has placed the research focus on hydrogel 3D printing for biomedical applications. **Figure 2a** shows components of a DLP platform [43] designed for making injectable hydrogel constructs with the incorporation of live cells for ocular stem cell transplantation. Their platform utilized a high-intensity UV light source (365 nm at ~88 mW/cm^2) together with several projection lenses to pass a collimated array of light through a photomask provided by the DLP device. They transferred the patterned light on top of a stationary printing stage. In this DLP platform, UV exposure at around 30 s was sufficient to be formed at a single step of about 18 injectable gelatin methacrylate (GelMA) based microscale cylinders of ~ 500 µm in diameter and ~ 500 µm in height (layer thickness). Ma et al. [43] used a similar platform. These custom-built optics and light sources enabled printing a thin layer of liver on a chip model with around 30 µm resolution in several seconds. Zhu et al. [49] used an almost similar DLP platform but replaced its light source with a near UV (405 nm) light source and added a moving stage in the *z-direction*. The new design successfully constructed more complex 3D hollow constructs such as tubes and nerve guidance conduits. A miniaturized DLP platform with a similar conceptual design enabled *in vivo* fabrication of hydrogel constructs under a near-infrared light [51]. Owing to the high penetration depth of the near-infrared light, the portable platform provided noninvasive treatments by fabrication of hydrogel structures under an animal skin [51]. These studies lack the multi-material capacity, which is considered in the following reports.

Grigoryan et al. [53] proposed a semiautomatic approach to change the material and manual washing of the construct under print in a DLP platform. **Figure 2b** illustrates the components of a platform proposed by Miri et al. [2]. They enabled fully computerized multi-material 3D printing in DLP platforms by adding a microfluidic chip. The platform allows the rapid exchange between different polymer inks in the vat area with computerized pneumatic controllers. A set of biconvex and planoconvex lenses and UV (380 nm) light of 100 mW/cm^2 intensity on the vat area on a microfluidic chip were sufficient to print parallel lines. Depending on the used optics and hydrogel system, these lines had a 25 µm resolution in 2D printing at exposure times between 1 and 20 s per layer. This advancement demonstrated an ultrafast and fully computerized DLP platform enabling 3D printing of multi-materials, co-culture of different cell lines, and fabrication of tissue building blocks for regenerative medicine applications. Demonstration of the scalability and resolution adjustment are other challenges in designing DLP platforms.

You et al. [54] introduced flashing photopolymerization to improve resolution in DLP platforms, in which light was exposed in millisecond scale (*flash*) portions. The approach attenuated light scattering and increased the crosslinking resolution. Xue et al. [55] controlled a scaffold's thickness with less sophistication through appropriate light power and exposure time selection. They showed that a predefined thickness of PEGDA solution between a glass slide and a coverslip could be crosslinked by a 2D light pattern projected through a plano-convex lens onto the solution (**Figure 2d**). UV light (365 nm) of intensity as low as 2.7 mW/cm^2 at 2.6 s of exposure was enough to fabricate their structure with a tailored thickness. The projection ratio and resolution of the light pattern were adjustable via the relative position of the plano-convex lens placed between the DMD chip and the polymer vat. Results demonstrated that by changing light input parameters and lens distances, one can reach good scalability and resolution adjustment. This may require developments in the design of tunable optical tools.

Regehly et al. Field [27] recently introduced another advancement in designing specific optics and suitable ink formulation for DLP platforms. They introduced Xolography, a recent state-of-the-art volumetric DLP printer that demonstrates a high-volume generation rate and a resolution about ten times faster than lithography. Integrating a benzophenone type II photoinitiator into a spiropyran photoswitch, a dual color photoinitiator (DCPI) system is developed for activation through simultaneous irradiation at two different light wavelengths. A thin light sheet of a first wavelength (375 nm) excites a thin layer of photoinitiator molecules from the initial dormant state to a latent state with a finite lifetime (approximately 6 s). To provide a homogeneous light intensity in the soft sheet, the light is divided and irradiated by the bioink volume from both sides of the material cuvette (**Figure 2e-i**). An orthogonally arranged DLP projector generates light of a second wavelength (550 nm). It focuses the sectional images of the 3D model on being manufactured into the plane of the thin light sheet. Those initiator molecules in the latent state absorb the patterned light reflected by the DLP projector and cause the current layer to polymerize (**Figure 2e-ii**). The desired object is continuously fabricated by projecting a sequence of images during synchronized movement of the ink volume through the fixed optical setup. The term xolography is used since the crossing (X) light beams generate the entire (holos) object using this printing process. The technology can be expanded to produce microscopic and nanoscopic objects using optical systems with a higher numerical aperture due to the irradiation with two light beams of different wavelengths at a fixed angle. This volumetric two-color 3D printing is based on molecular photoswitches and does not require any nonlinear chemical or physical processes. It is expected that Xolography will stimulate 3D printing research fields from photoinitiator and material development to projection and light sheet technologies for rapid and improved-resolution 3D printing in the near future. The approach's success is strongly dependent on the development of materials that can be used in this system, enabling controllable gelation using a specific dual-color photoinitiator system.

In summary, the main advantage of DLP printing is its high speed for fabricating complex structures. The main challenges are (i) difficulty in combining different materials (multi-material printing) that can be solved by using microfluidic setups, and (ii) difficulty in adjusting printing resolution that can be solved by proper choice of optical hardware and light patterning techniques such as flashing photopolymerization to reduce light scattering, and (iii) difficulty to develop proper ink materials and photoinitiator systems for DLP platforms. This can be addressed by introduction of novel formulations composed of molecular photoswitches and the light sheet technology. In the next section, we summarize the versatility in the design of optics for different DLP platforms. Then we review the solution of kinetics equations for the photopolymerization reaction. These equations will address phenomenological relationships between governing design parameters in DLP platforms.

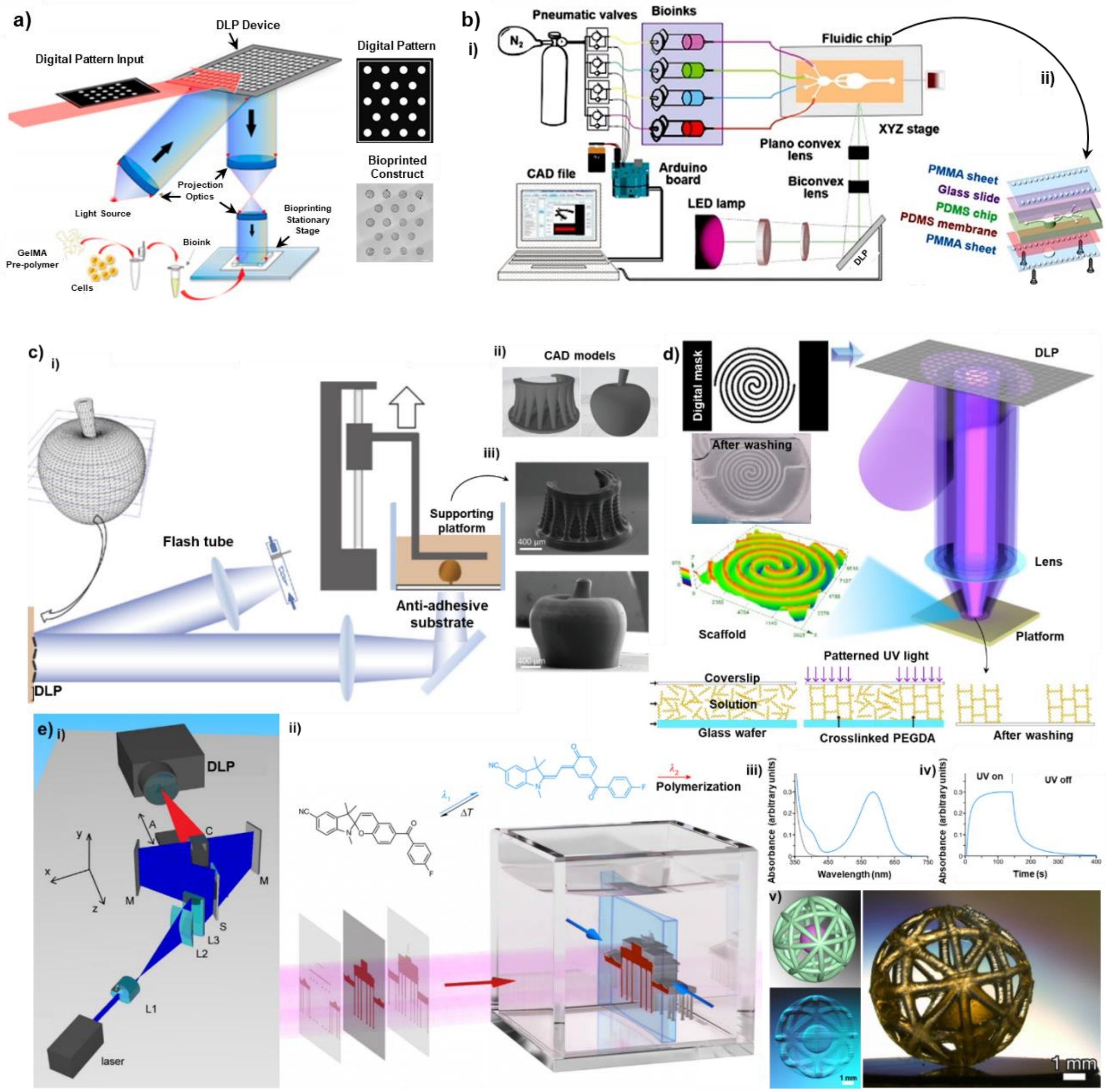

Figure 2. The advancements in DLP platforms: a) Rapid printing of conjunctival stem cell micro constructs in 18 cylindrical shapes for subconjunctival ocular injection, [56], b) Microfluidics enabled multi-material maskless DLP 3D

printing [2]. c) Flashing photopolymerization 3D printing, i) Schematic diagram of the printer, ii, iv) 3D models of a micro altar and micro apple, iii,v) SEM image of the printed models by flash photopolymerization with 100 µm layer thickness [54], d) Projection-based 3D printing of cell patterning scaffolds with multiscale channels [55], e) Xolography linear volumetric 3D printing, i) diagram of xolography and the thin light sheet intensity distribution, ii) Rendered illustration of the printing zone and associated photoinduced reaction pathways of the DCPI, iii) Absorbance spectrum of DCPI under dark conditions (grey) and 375 nm UV irradiation (blue), iv) photoswitch kinetics probed at 585 nm, v) the model, ink under 3D printing and the fabricated part which is a spherical cage with free-floating ball [57].

3.2. Optical Design Parameters

Table 1 shows a variety of DLP platforms based on different optics, light source specifications, obtained resolutions, and speeds. A wide range of wavelengths is successfully used in DLP platforms. The range starts from the UV range ($\lambda = 320$ to 400 nm), passes through the visible range ($\lambda = 400$ to 700 nm), and reaches up to near-infrared light ($\lambda = 800$ to 1000 nm). By increasing the light wavelength, the lower energy characteristic of the light and inadequate light absorption by the initiators can challenge the photopolymerization reaction needed to print a robust structure. Generally, increasing the wavelength from UV to infrared light decreases printing resolution (see **Table 1**). Separate from the wavelength, proper setting of all other optical parameters such as collimation and polarization of the light is needed to achieve a balance between resolution, light penetration depth, and speed of 3D printing. Selection of a proper photoinitiator system, light intensity, and exposure time allows us to achieve a improved printing resolution and printing speed. For instance, in Ru:SPS photoinitiator system, a light intensity as low as 0.23 mW/cm^2 and 30 s exposure time can be used to achieve ~ 50 µm resolution at 10-100 µm/s vertical speed in DLP 3D printing. If LAP is incorporated in the ink composition instead of Ru:SPS, a light intensity as large as 700 mW/cm^2 and 200 milliseconds exposure time can be used to fabricate features of ~ 15 µm resolution at 40 µm/s vertical speed. The photoinitiator's molar absorptivity (or extinction coefficient, ε) can describe these observations. Photoinitiator Ru:SPS shows a high molar absorptivity ($\varepsilon = 14600$ M^{-1}cm^{-1} at 450 nm) approximately 300 folds higher than that of *LAP* ($\varepsilon = 50$ M^{-1}cm^{-1} at 405 nm) [58]. Ru:SPS can be used for photocrosslinking at much lower light intensities than LAP because a higher molar absorptivity leads to a higher photo reactivity.

In cell printing, enhancing light energy by decreasing the wavelength can generally increase the printing resolution at the expense of lower cell viability since high-energy UV light is a potential source of damage in DNA, affecting the proliferation and fate of live cells. DLP is considered a contactless printing method, showing reasonable cell viability at most platforms reviewed in **Table 1**. Contact-based 3D printing methods such as extrusion printing apply shear forces to the bioink, potentially damaging the cell membrane and decreasing viability. Contactless DLP printing has become a popular modality because of its higher fabrication speed (100-1000 mm^3/s) and improved resolution (< 20 µm) compared to other printing methods. **Table 1** reveals that most currently developed platforms ignore the potential of grayscale 3D printing. This capability can be incorporated into a DLP platform without increasing the hardware costs. Grayscale 3D printing technique allows controlled gradient crosslinking in printed structures and can bold 4D printing capabilities. Conceptually, 4D printing means introducing programmable time-dependent material properties to a final 3D printed product using a stimulus, for instance, upon exposure to different wavelengths of light [59] or submerging it in a medium to trigger a programmed swelling response [7]. In the last section, we categorized different types of 4D printing stimuli in DLP platforms as future trends (**Table 4)**.

In summary, enhancing the light energy by decreasing the wavelength can increase the printing resolution. The role of photoinitiator content, molar absorptivity, light intensity, and exposure time on printing resolution is more complex. The following section is devoted to introducing different types of light-material interactions. We summarize the solution of kinetic equations for curing reaction to elucidate the non-linear dependence of the curing depth on the photoinitiator content, its molar absorptivity, light intensity, and exposure time during DLP printing.

Table 1. Versatility of optics design in DLP printing platforms

Initiator	Optics Characteristics			DLP Chip	Grayscale	DLP Output			
	λ (nm)	I mW/cm^2	t (s)	H*W pixels		Cell Viability	Planar Resolution (μm)	Vertical Speed (μm/s)	Ref.
UCNP@ LAP	980	-	15	1024× 768	No	>80% in 7 days	100	13	[51]
Eosin Y	400-700	-	240	1920 x 1080	No	60-85% in 5 days	50	~5	[52,60]
LAP	405	16	120	1280 × 800	No		50	-	[53]
LAP	405	7-17	10	2560× 1600	No	High viability in 11 weeks	10	400	[49]
LAP	405	22	6-120	1920 x 1080	No	High viability in 14 days	10	-	[61]
LAP	365	500	1-20	1050× 920	No	>80% in 7 days 30 days	10	5-100	[2]
LAP	365	88	15	-	No		50	20	[62]
LAP	365	88	10-30	1024× 768	No	70% in 10 days	30-50	15-50	[43,56,63]
LAP	365	11	45	1920 x 1200	No	42-60% in 3 days	~ 25	5-15	[64]
LAP	385	-	30	912x1140	No	50%- 90% in 1 day	50	~10	[65,66]
LAP	365	2.7-6	3	1920x1080	No	High viability in 2 days	20	~ 250	[55]
Ru:SPS	400-700	0.23	30-60	954 × 480	No	>98% in 14 days	50	10-100	[67]
LAP	980	-	15		No	High	>100	-	[51]
LAP	380	700	0.2	-	No	-	15	40	[6]
LAP	365	2.8-5.6	5	2560 × 1600	No	Not applicable	<10	~ 20	[54]
DCPI	520 + 375	215	<1	3840 × 2160	No	Not applicable	20	140	[57]
BAPO	405	3-10	10	1920 × 1080	No	Not applicable	<100	8-12	[1]
Irga 819	380	18	30	1280 × 800	**Yes**	Not applicable	>50	3	[7]

*** λ: light wavelength; I: Intensity of light off the lens; t: light exposure time; NA: not applicable; "-": not enough data to report. UCNP@ LAP: up-conversion nanoparticle coated with LAP as photoinitiator; BAPO: bis-acylphosphine oxide; DCPI: dual color photoinitiator.**

4. Light-Material Interactions

In the DLP 3D printing process, light refracts when it travels from the DLP source and reaches the ink material which presents another refractive index (**Figure 3a**). The refractive index of the ink material determines the speed of light propagation and phase. Reflection happens when the light is reflected on the surface of the ink material because of the difference between the refractive index of the ink material and air. **Figure 3** shows the main parameters that should be considered when designing a DLP printing setup. Scattering is an important phenomenon that affects the resolution.

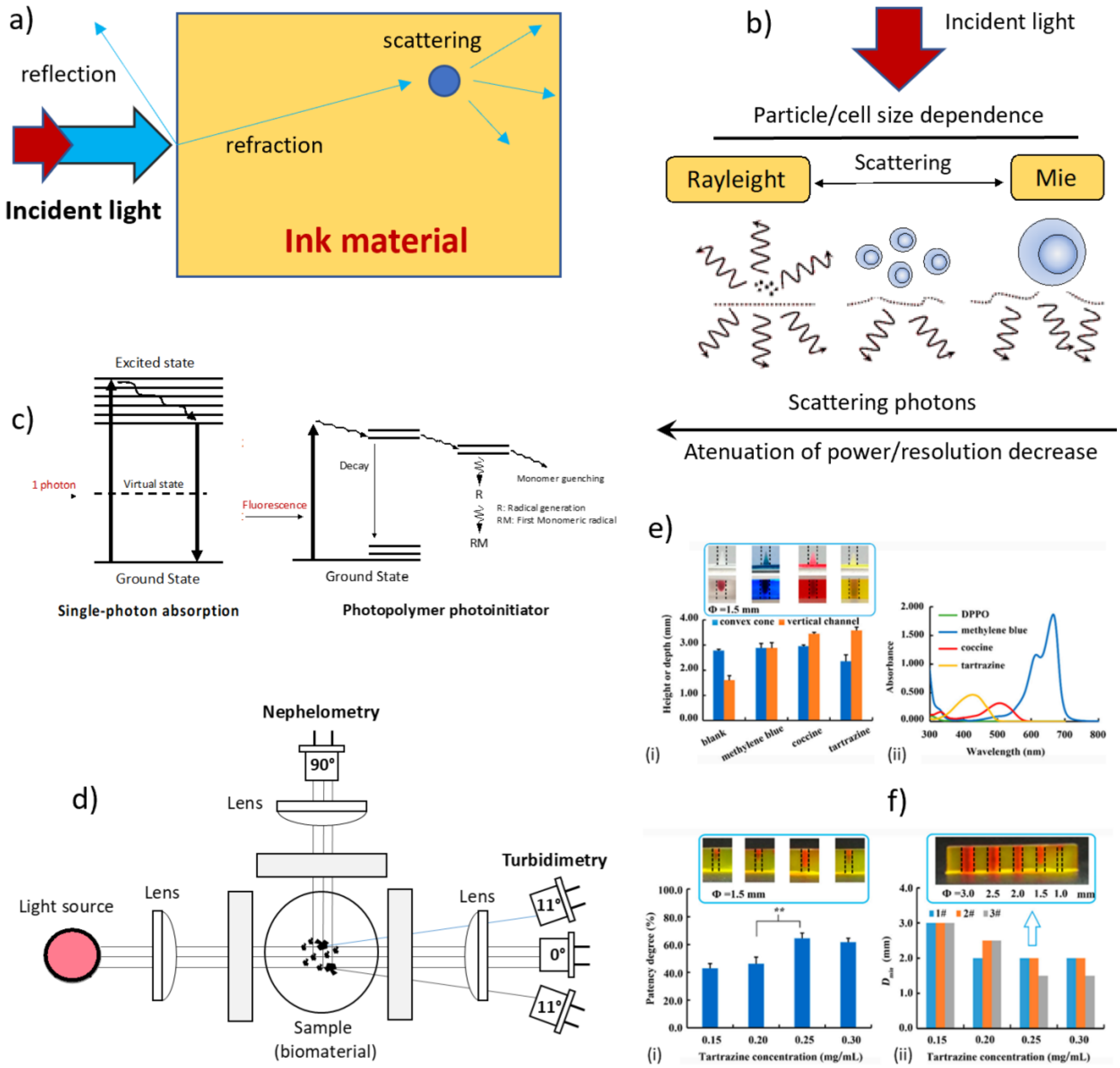

Figure 3. Light-material interactions: a) Diagram of basic concepts; b) Single photon absorption process; c) Sketch of particle size effect on scattering; d) Diagram of the two primary methodologies to measure scattering in an ink material; E) Effect of different photo absorbers (i.e., methylene blue, coccine, and tartrazine) on the printability of convex cone and vertical channel; (i) Wavelength scan results of the photoinitiator (i.e., Diphenyl (2,4,6-trimethylbenzoyl) phosphine oxide, DPPO) and photo absorbers; f) Effect of tartrazine concentration on (i) Patency degree of the vertical channel with a diameter of 1.5 mm, and (ii) The minimum printable diameter (D_{min}) of the vertical channel with different diameters, and typical sample with 0.25% tartrazine [68].

4.1. Scattering Types and Measurements

Scattering occurs due to loss of directionality of light and spread of light beam spot. This phenomenon controls fair intensity distribution in the ink material. Light scattering can be defined according to the sizes of particles/molecules/cells in the ink composition. Mie scattering occurs when particles are the same size as the wavelength of light. Rayleigh scattering occurs when particles are much smaller than the wavelength [69,70]. **Figure 3d** illustrates two techniques that can be used to measure light scattering in an ink material. The first technique is turbidimetry, in which light scattering is determined by measuring the decrease in intensity of the light beam after passing through the ink material. The second technique is nephelometry, in which light scattering is determined by measuring light at an angle (usually 90º) away from the incident light passing through the ink material (**Figure 3d**).

4.2. Scattering Inhibition Methods

Achieving improved resolutions in DLP 3D printed constructs with light scattering problems has remained a technological challenge. To overcome resolution deterioration due to light scattering in hydrogel 3D printing, You et al. [54] developed a DLP method called flashing photopolymerization (FPP). In contrast to conventional DLP platforms where light is exposed continuously, in flashing polymerization light exposure to the vat is applied in millisecond scale *flash* portions. Since the flash exposure, the prepolymer negligibly scatters light; the polymerization takes place without penetrating continuous light into the environment. This leads to the exposure pattern being less perturbed by light scattering. **Figure 2c** shows the schematic diagram and resolution of prototypes constructed with this technique. Implementation of machine learning approaches in 3D printing is another strategy successfully used in developing improved resolution DLP printers. You et al. [33] have developed a sophisticated neural networks algorithm to control light-material interactions to mitigate the scattering effects, especially in sharp corners of the models in a DLP printer.

Another strategy to control the scattering effects is the addition of photo absorbers which work like light attenuators by absorbing excess light, which improves the pattern fidelity. Several researchers have reported some forms of light absorption or polymerization inhibition to reduce scattering, resulting in more accurate features. Zissi et al. [71] theoretically and experimentally showed that cure width and cure depth could be decreased using a photo absorber, and these effects were established as a function of the concentration of the photo absorber in the ink solution. The quality of a 3D printed structure is related to the curing properties of each layer. It is essential to acquire insight into the relationship between the photo absorber composition, gelation kinetics for the layer formation, and its mechanical properties. Khairu et. al [72] used a photo absorber (Sudan I) to effectively control UV penetration for fabricating 3D microstructures in UV micro stereolithography. Yan Yang et. al [68] evaluated the impact of various photo absorbers (i.e., methylene blue, coccine, and tartrazine) over the photocuring process and printing fidelity (printability of convex cone and vertical channel). With the highest absorbance at 405 nm, tartrazine was the most effective photo absorber in slowing down the photocuring reaction. As illustrated in **Figure 3e-i**, the height of the printed cone (Φ = 1.5 mm) was not different after adding methylene blue or coccine. By adding tartrazine, the height of the cone decreased, which revealed that tartrazine was able to slow down light-induced crosslinking reaction. The depth of the internal vertical channel (Φ = 1.5 mm) increased after tatrazine was added as a photo absorber, enabling minimization of light scattering into the channel. This slowed down the overturning of the nonprinted area and allowed the printability of internal structures. This improvement in printing accuracy of the inner channel was related to the absorption of light scattering into the channel by tartrazine [68]. Grigoryan et al. demonstrated that adding tartrazine in PEGDA hydrogels can decrease light scattering for improved-resolution fabrication of an alveolar model topology with a voxel resolution of ~ 5 µm with perusable open channels measuring as small as 300 µm in diameter [42].

Adding inorganic gold nanoparticles, which are biocompatible for tissue bioprinting, has also been reported as a viable strategy to attenuate light scattering. By controlling the diameter of the nanoparticle, the peak absorbance can also be controlled [73]. The interaction between light and spherical nanoparticles can be described using the Mie theory [74]. Mie theory calculations determine the theoretical absorption and scattering cross sections, the sum of which is equal to the total extinction. This can be used to predict light scattering during DLP printing.

4.3. Light Absorption Photo-Chemistry

Photopolymerization includes the reaction of monomers that creates large networks once irradiated with UV light via the chemical absorption of photons. Absorption is regulated by Beer's law, mainly when using monochromatic beams [31]. It correlates this absorption to the wavelength of the incident light. With I_0 being the intensity of the radiation that enters the ink material and I the power of the radiation that goes across, the transmittance T is given by $T= I/I_0$. Beer's law can be expressed as:

$$log_{10}\left(\frac{\mathrm{I}}{\mathrm{I}_0}\right) = abc \qquad (1)$$

Where b is the thickness of the box, c is the concentration of the sample in the solution and a is the capacity of the sample to absorb radiation. Beer-Lambert law can be simplified to A= abc, where A is the absorbance and is expressed as:

$$\mathrm{A} = \mathrm{abc} = \log_{10}\left(\frac{\mathrm{I}}{\mathrm{I}_0}\right) \qquad (2)$$

Beer's law says that the concentration and the absorbance are linearly proportional (for a constant thickness and radiation wavelength). Consequently, the dispersion/scattering and absorption are conditioned by the wavelength and the increase in the blue region of the electromagnetic spectrum compared to the red and infrared regions. This absorption can be aroused by the reactant monomer or by a photoinitiator's transference of absorbed energy. When photoinitiators are exposed to light, they generate free radicals which react with monomers and oligomers and initiate the polymer chain reaction and growth. Photoinitiators are vital elements for photocrosslinking in DLP printing [75].

4.4. Photopolymerization Kinetics

The equations derived in the **Supplementary Material** show the role of photoinitiator concentration, its extinction coefficient, exposure time and light intensity on curing depth in a DLP printer. **Figure 4** shows that there exists an optimal photoinitiator concentration (a threshold concentration) in the ink formulation to achieve the highest curing depth during printing each layer.

The optimal photoinitiator concentration nonlinearly decreases with increasing light intensity (**Figure 4a** and **Eq. S10**) and increasing exposure time (**Figure 4b** and **Eq. S10**). Increasing light intensity beyond a conventional range is limited by access to costly powerful LED/light sources. Increasing the exposure time is easily accessible through programming the DMD chip. However, it decreases the speed of printing. In layer-by-layer 3D fabrication, both the exposure time and the curing depth of each layer determine the speed of 3D printer. Redundant intensity, exposure time, and photoinitiator concentration give raise to light scattering, leading to overcuring and deteriorated resolution. More details are discussed in **Supplementary Material's** section about calculations of the optimal photoinitiator concentration in a DLP setup. In summary, engineers have to consider the light-matter interaction equations including fabrication parameters and ink material variables to control the printing quality when setting optimal conditions for a DLP platform. Next section is devoted to providing a deeper insight about the chemical properties and molecular structure of inks used in DLP platforms.

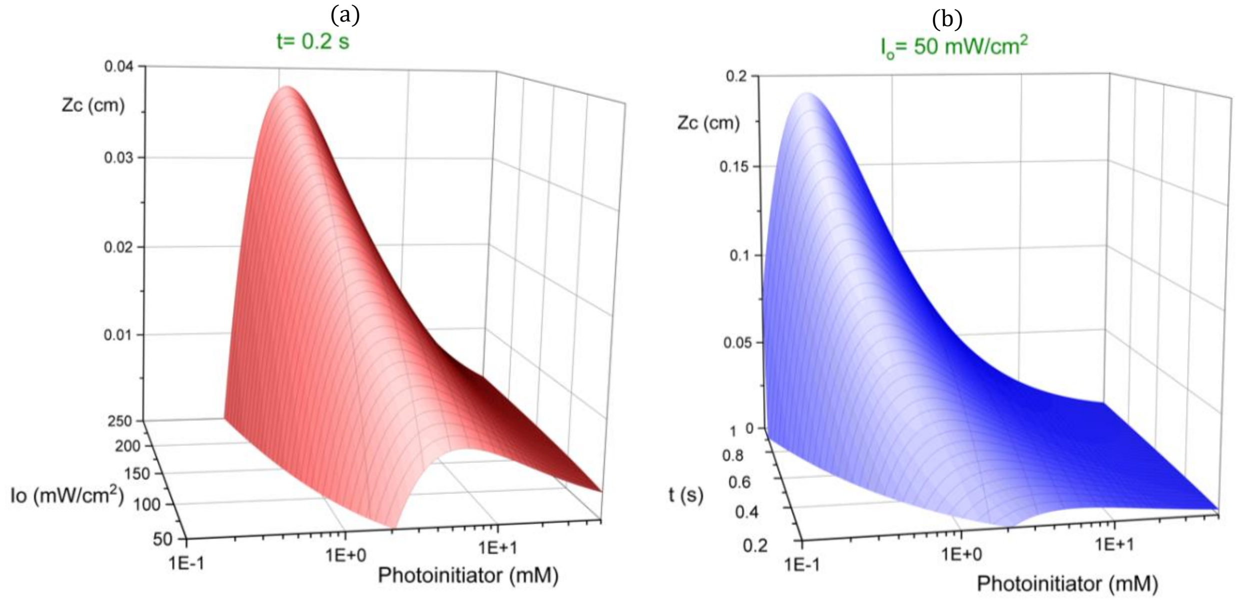

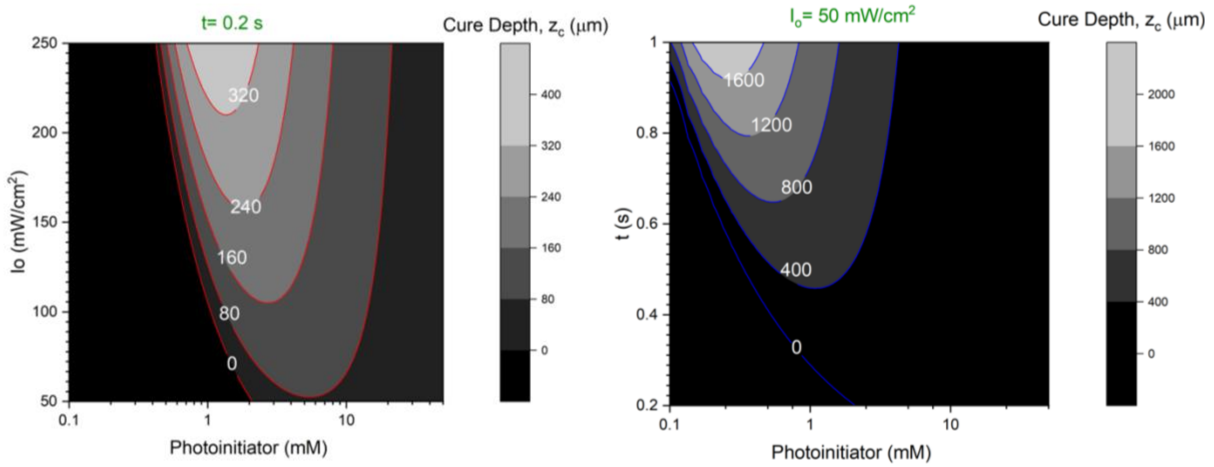

Figure 4- 3D curves and relevant 2D contour plots to address the dependence of the curing depth on the photoinitiator concentration and (a) the light intensity at fixed exposure time, t=0.2 s, (b) the exposure time at fixed light intensity, $I_0 = 50\ \frac{\text{mW}}{\text{cm}^2}$, in a DLP printing platform. The ink chemical properties (α and ϵ parameters) obtained from Lee et al. [76].

5. Ink Selection

5.1. General Guidelines

Table 2 summarizes the main compositions used as an ink material to benchmark DLP platforms. PEGDA of molecular weight between 250 and 700 Da at concentrations between 10 to 50 % v/v in water is a widely used material to demonstrate the potential of a DLP platform for improved resolution printing. To test cell printability, PEGDA cannot be of use since cells show not enough attachment to PEGDA scaffolds. Alternative material for testing cell printability in a DLP platforms is GelMA of concentration between 5 to 15 % w/v. GelMA provides a lower printing resolution owing to a lower concentration of polymer content, higher molecular weight of the polymer, and higher light scattering, compared to PEGDA. Due to improved cell attachment to gelatin macromers, GelMA is more useful to conduct cell studies with DLP platforms. Mixing PEGDA with GelMA can lead to a balanced printing resolution and cell attachment. The hydrogel constructs fabricated by these polymers are relatively brittle. Chitosan methacrylate (CHI-MA) hydrogels in presence of LAP as a photoinitiator and blue light (405 nm) are attractive alternatives owing to their enhanced mechanical properties, tailorable grafting degree, biocompatibility and biodegradability [77].

Depending on the application, some studies incorporate other inks such as HAMA, SF-GMA, SF-PEG4A PVA-MA, or BPADA-GMA-BA [2,7,43,56,58,62,63,67]. To achieve biocompatibility, it is necessary to use cell friendly photoinitiator systems such as Ru:SPS or LAP [4]. Depending on the wavelength of the light source, several dyes as shown in **Table 2** can be incorporated into the bioink formulation for absorbing the scattered light and increasing printing resolution. The largest and the smallest size of features already printed by different DLP platforms are shown in **Table 2**. Most of DLP platforms are capable of printing large features of centimeter size scale in one-time exposure. This is considered large enough for additive manufacturing of industrial models and tissue building blocks. The smallest printable feature size fits in a wide range between 10 μm and 500 μm, depending on both ink material composition and the particular optic design used for the DLP platform.

In summary, PEGDA is helpful to test the resolution of printing 3D structures, while GelMA and HAMA are useful to test cell compatibility of the platform to print cell laden hydrogel constructs. These 3D printed hydrogels mostly show brittleness and low mechanical properties. To test potentials of the platform to print constructs of stronger mechanical properties CHI-MA, PVA-MA, SF-GMA and SF-PEG4A are candidate biomaterials. PETA and BPADA-GMA-BA provide much higher mechanical properties at the cost of losing biocompatibility in product.

Table 2. Common ink compositions for DLP printing

Ink	Initiator	Absorber	Feature size	Biocompatibility	Ref.
GelMA (15%w/v)	UCNP@LAP	No Dye	150 μm- 1 cm	High	[51]
CHI-MA (1 %w/v)	LAP	No Dye	50 μm- 1 cm	High	[78]
CMC-MA (2 %w/v)	LAP	No Dye	100 μm- 1 cm	High	[79]
SF-GMA (10-30 %w/v)	LAP	No Dye	100 μm- 3 cm	High	[80]
SF-PEG4A (2 %w/v)	Eosin Y	No Dye	500 μm- 1 cm	High	[81]
PVA-MA (10 %w/v), PEGDA (40 %v/v)	Ru:SPS	Ponceau-Red	500 μm-1 cm	High	[58,67]
GelMA (10 %w/v), PEGDA (10 %v/v)	Eosin Y	A Food Dye	500 μm-1 cm	Medium	[52,60]
PEGDA (25 %v/v)-GelMA (7.5 %w/v)	LAP	No Dye	100 μm-5 cm	High	[49]
PEGDA (20 %w/v)	LAP	Tartrazine (Organic dye)	100 μm-3 cm	High	[61]
HAMA, GelMA (20 %w/v)	LAP	No Dye	200 μm-6 mm	High	[65,66]
BPADA-GMA-BA (69:23:8)	Irga819	Sudan I	200 μm-6 mm	NA	[7]
GelMA-PEGDA	LAP	A Food Dye	15 μm-2 cm	Low	[6]
PEGDA (20 to 50 %v/v), GelMA (5%w/v)	LAP	No Dye	100 μm-2 mm	Medium	[54,55,64]
GelMA-PEGDA (10 %w/v), GelMA (2.5%w/v)-HA (1 %w/v), GelMA (10%w/v)-GMHA (1%w/v)	LAP	A Food Dye	10 μm-5 mm	Medium	[2,43,56,62,63]
PETA (95 %w/v)	DCPI	No Dye	20 μm-5 cm	NA	[57]

NA: not applicable; UCNP @ LAP: LAP coated on an Up-Conversion Nano Particle; GelMA: gelatin methacrylate; CHI-MA: chitosan methacrylate; CMC-MA: carboxymethyl cellulose methacrylate; SF-GMA: silk fibroin produced by a methacrylation process using glycidyl methacrylate; HAMA: hyaluronic acid methacrylate; PVA-MA: poly-vinyl alcohol methacrylate; PEGDA: Polyethylene Glycol Diacrylate; SF-PEG4A: silk fibroin (SF) incorporated 4-arm polyethylene glycol acrylate; BPADA: bisphenol A ethoxylate diacrylate; GMA: glycidyl methacrylate; BA: n-butyl acrylate; PETA: pentaerythritol tetraacrylate.

5.2. Classification of Ink Molecular Structures

A DLP printing ink is mainly composed of a mixture of monomers including functional groups (mostly acrylate or vinyl), a light sensitive initiator and, when needed, a photo absorber. Correct choice of fillers in the photocurable ink formulation allows to tailor functional properties for the printed constructs. Molecular structures of main monomers used as a DLP printing ink are classified and illustrated in **Table 3**. Most of DLP printrs make use of inks comprised of a sort of acrylate functional group in their molecular structure. Other ink formulations which implement thiol or thiol–acrylate based vitrimers mostly need toxic photoinitiators, their applications are excluded here and discussed elsewhere [82,83]. In ink molecular structure, acrylate functional groups can show up as either a repeating side group (i.e., pendant) or as an end-group (i.e., termination).

5.2.1. Pendant Formulations

Examples of monomers with acrylate pendant groups, are gelatin methacrylate [51], chitosan methacrylate [78], carboxymethyl cellulose methacrylate [79], hyaluronic acid methacrylate [65,66,84], poly-vinyl alcohol methacrylate [44], and silk fibroin produced by a methacrylation process using glycidyl methacrylate [80]. Majority of these inks show good water solubility, low toxicity, and biocompatibility. Their monomer molecular weight is in a wide range between 18’000 Da and 300’000 Da, while the obtained resolution during DLP printing is almost non relevant to the monomer molecular weight (**Figure 5e**). Increasing the substitution of acrylate as a side group on the backbone of the monomer (i.e., conversion ratio) can increase DLP printing resolution.

5.2.2. Termination Formulations

Examples of monomers which use acrylate as a terminal group include polyethylene glycol diacrylate [61], bisphenol A ethoxylate diacrylate [7], diurethane dimethacrylate [57], and silk fibroin incorporated 4-arm polyethylene glycol acrylate [81]. Here, small size monomers such as pentaerythritol tetraacrylate [57], hydroxyethyl methacrylate [57], dimethyl acrylamide [1], trimethylolpropane triacrylate [1], isobornyl acrylate and acryloylmorpholine [85] can also be implemented. These monomers together with a proper photoinitiator [4] are successfully used as an ink in DLP platforms. Increasing the monomer molecular weight decreases the density of acrylate per volume of the ink which reduces the resolution of DLP. For instance, in PEGDA where acrylate is used as termination it is expected that decreasing the molecular weight of PEG increases the acrylate density and increases DLP printing resolution. We showed this phenomenon in a macroscopic scale in **Figure 5c-i** for PEGDA 6000 Da (impaired resolution) and **Figure 5c-ii** for PEGDA 700 Da (improved resolution) where similar photoinitiator content and exposure time is applied to print both samples at 12.5% w/v polymer content.

Table 3. Molecular structure of DLP printing inks

Ink	Molecular Structure	Monomer Mw (Da)	Feature Size	Water Solubility	Ref.

Acrylate as pendant (a repeating side group)	GelMA (15% w/v)	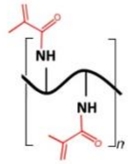	20’000	<150 μm	High	[51]
	CHI-MA (1% w/v)	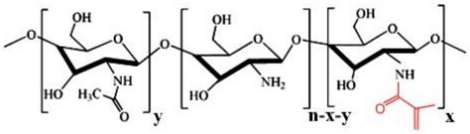	~300’000	50 μm	High	[78]
	CMC-MA (2% w/v)	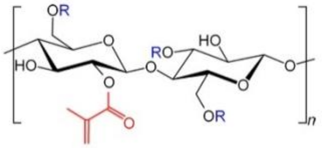	250’000	100 μm	High	[79]
	SF-GMA (10-30% w/v)	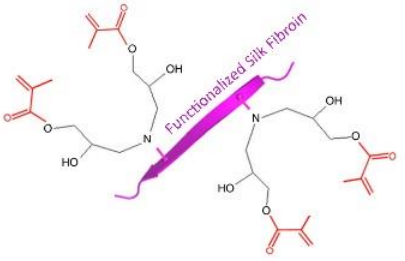	~300’000	100 μm	High	[80]
	HAMA (1-2% w/v) (viscosity: 3.9-12.8 mPa.s)	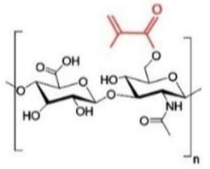	120’000	<200 μm	High	[65,66]
	PVA-MA (10% w/v) (viscosity: 12.5 mPa.s)	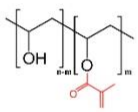	~18’000	<100 μm	-	[44]
Acrylate as termination (an end-group)	PEGDA (20% w/v)	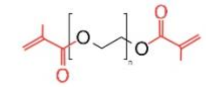	575,700, 4’000, 6’000	220-500 μm	High	[Here]
	SF-PEG4A (4% w/v)	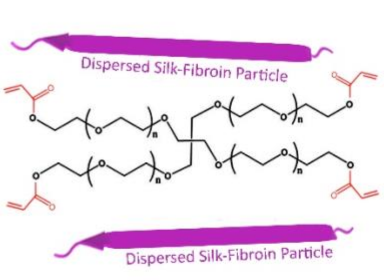	20’000	~500 μm	-	[81]

BPADA-GMA-BA (69:23:8)	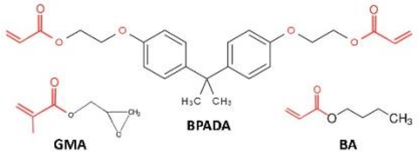	425-142-128 (~336)	120 μm	Limited	[7]
PETA, UDMA-HEMA (10:1)	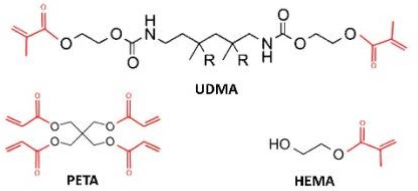	352, 470-130	- (~25 μm with Xolography)	Limited	[57]
DMA-TMPTA (4:1)	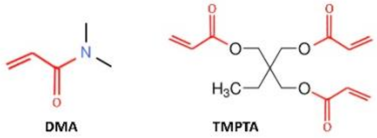	99-296 (=138)	~80 μm	Limited	[1]
IBOA, ACMO (viscosity: 20 mPa.s)	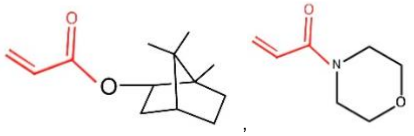	208, 140	-	Limited	[85]

'-': not enough data reported with a DLP platform comparable to other studies; Mw: molecular weight; UDMA: diurethane dimethacrylate; HEMA: 2-hydroxyethylmethacrylate; DMA: dimethyl acrylamide; TMPTA: trimethylolpropane triacrylate; IBOA: isobornyl acrylate; ACMO: 4-acryloylmorpholine.

5.3. Role of Monomer Molecular Weight

There is no systematic study, which reveals the role of monomer molecular weight on printing resolution in DLP platforms. Printing resolution depends on both the design of optics and the characteristics of the ink material. As a rough estimation for almost similar DLP platforms, in **Figure 5e** we tried to plot the resolution (i.e., the minimum width of lines printed with DLP) versus the average monomer molecular weight based on both data summarized in **Table 3** and our own measurements on PEGDA samples with different molecular weights. We used a 'parallel lines' photomask with varying width from 1 pixel to 30 pixels keeping the distance between white lines same as the line width (see **Figure 5d-i**). We used a custom-built DLP platform to print PEGDA (20 wt.%) with different molecular weights (575, 700, 4000 and 6000 Da). For instance, **Figure 5d-ii** show two printed patterns obtained by optical microscopy. **Figure 5d-iii** shows the result obtained by fluorescent microscopy where the resolution of printing (narrowest printable line) is clearly obtained. Results of experiments on PEGDA of diverse molecular weight are provided as supplementary data (**Table S1).** These experiments together with the data in Table 3 are used to illustrate **Figure 5e.** This figure implies that if acrylate is used as termination, the minimum printable feature size is increased proportional to the average of monomers molecular weight. Indeed, by increasing the molecular weight the relative density of acrylate groups compared to uncrosslinkable polymer content will decrease. More importantly, by increasing the molecular weight the light scattering increases due to presence of larger macromolecules which enhances Rayleigh scattering and decreases the resolution of printing. **Figure 5f** illustrates the results of dynamic light scattering (DLS) performed on uncrosslinked PEGDA. The results clearly show that increasing the molecular weight forms larger nanometer size particles with higher population (i.e., intensity) which consequently enhances the light scattering. Note that **Figure 5f** is devoted to particle sizes much smaller than the DLS laser light wavelength, ca. 200 nm. Here, increasing the particle size by increasing the molecular weight enhances the Rayleigh scattering and decreases the printing resolution. **Table 3** showed that in majority of cases if monomer molecular weight is above approximately 20’000 Da, acrylate is used as a pendant in ink formulation. **Figure 5e** implies that in this situation the minimum printable feature size is irrelevant to the monomer molecular weight. **Figure 5g** summarizes this information by providing a decision tree to assist enhancing DLP printing resolution based on the ink molecular structure.

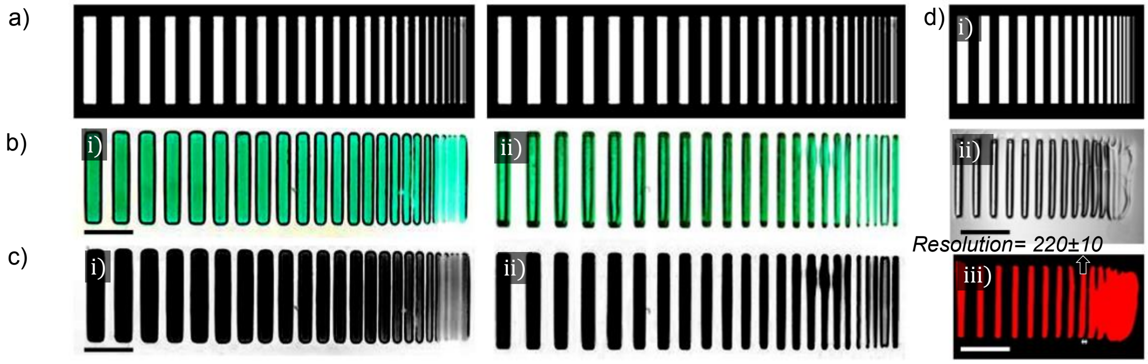

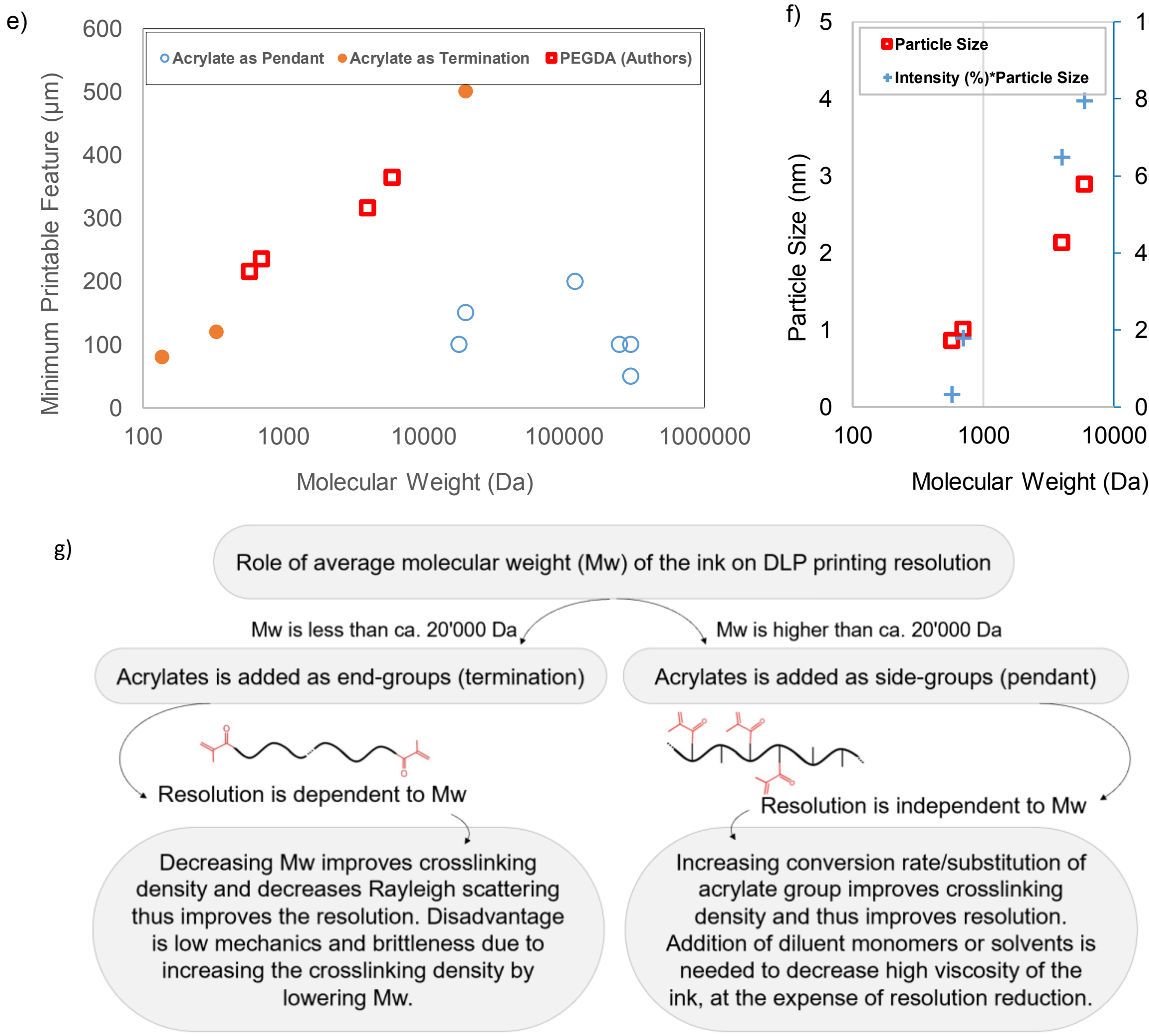

Figure 5. Role of molecular structure on obtained resolution during DLP printing; a) used photomask for DLP printing of PEGDA; b) printed structures achieved from (i) PEGDA 6000 Da and (ii) PEGDA 700 Da (3 mM Ru:SPS), scale bar 5 mm; c) same patterns after removing background in grayscale mode; d) parallel lines photomask (i), obtained pattern under optical microscopy (ii), obtained pattern under fluorescent microscopy when Comarin 6 is used (iii) and the demonstration of estimated resolution based on the thinnest printable line, scale bar 1 mm; e) variations of the minimum printable feature size obtained from different formulations shown in **Table 3** and the authors measurements on PEGDA samples; f) particle size obtained by DLS for uncrosslinked PEGDA samples of different molecular weights where size of particles are much smaller than the laser wavelength, ca. 200 nm; g) decision tree to help improving resolution of DLP printing based on the ink molecular structure.

5.4. Role of Ink Viscosity

It is worth noting that the viscosity and solubility of some inks in the solvent significantly change by increasing their monomer molecular weight. For instance, by increasing the molecular weight of hyaluronic acid from 100´000 Da to 1´000´000 Da, the viscosity of HAMA at a fixed polymer content remarkably increases. To use the ink in a DLP platform, one should adjust the ink viscosity by decreasing polymer content (or increasing the solvent). This in turn decreases the acrylate density per volume of the ink and can reversely attenuate DLP printing resolution.

In summary, different DLP printing inks were categorized in this section considering the molecular structure of their monomers. In high molecular weight inks, acrylate or vinyl groups were mostly attached as a side group, pendant, to the backbone of molecular structure. Here, the density of acrylate groups remains constant by increasing the molecular weight; thus, no significant change was observed in obtained resolution during DLP printing. These formulations included GelMA, HAMA, CHI-MA, CMC-MA, SF-GMA, and PVA-MA. In low molecular weight inks, acrylate or vinyl groups mainly were attached as an end group, termination, to the backbone of molecular structure. Here, with increasing the molecular weight, the relative density of acrylate groups was reduced while light scattering was enhanced. Therefore, increasing molecular weight could decrease the printing resolution or increase DLP's minimum printable feature size. The next section represents future trends in DLP printing, including emerging techniques for multi-material and 4D fabrication.

6. Future Directions

6.1. Inks Enabling 4D Printing Mechanisms

One of the current trends in fabrication is creating dynamic constructs with time-dependent properties. According to the 4D printing concept [84,86], a 3D printed structure undergoes time-dependent self-transformation in shape, properties, or functionality when exposed to predetermined stimuli such as light [87], heat [7,88], magnetic field, or electrical field [89], humidity [90], and changes in pH [84,91]. **Table 4** summarizes the inks used for 4D printing, mainly in DLP platforms. Different mechanisms governing on 4D stimulation of DLP printed products are shown in **Table 4,** which can be classified into two main tools. One tool consists of thermally activated microstructural transformation. The thermally activated change can be due to the shape memory behavior of the DLP printed material [7,88,89] or due to microstructural evolution in a DLP printed polymer foam [92]. The next mechanism consists of humidity-activated transformation, including non-reversible shape transformation [84,90,91] or reversible color transformation [87] due to water content variations in the environment. It is advantageous if the polymer can demonstrate the reversibility of the 4D transformation, which is practically provided by physical/chemical crosslinking and a reversible stimulus. 4D printing is still in its infancy, and few ink formulations are recognized till now with potential *reversible* 4D applications in DLP platforms [87]. Implementing molecular motors or photoswitches such as azobenzene and arylazopyrazole [93] in the ink molecular structure is a promising future direction in 4D DLP printing because they provide tunable, time-dependent and reversible properties [94] to the printed samples after 3D printing.

4D printing typically intends to include significant shape transformations from the initially printed geometry to the final activated stage. To fabricate a complex structure, one should consider nonlinear mechanical modeling at large deformations to predict the final shape from the as-printed form of the system. Most polymers often exhibit nonlinear, visco-hyperelastic behavior. Functionality transformation is generally a time-dependent, transient process. Consequently, it is more challenging to define or quantify resolution in 4D printing than conventional 3D DLP printing. In hydrogel systems, 4D DLP printing is possible either through the capability of the ink for gradient crosslinking (to exploit the humidity-activated mechanism) or through an engineered gradient distribution of (nano-)particles during printing (to introduce a thermally activated tool). Till now, few ink formulations have been known to show good capability for gradient crosslinking at the molecular level toward the 4D printing [84,90,91].

Table 4. Inks developed for 4D printing with DLP platforms

Ink	4D Stimulation	Potential Applications	Example	Ref.
[Proprietary of Desktop Metal ™]	Heating up to 170 C for microstructure transformation	Industrial polymer foams for automotive	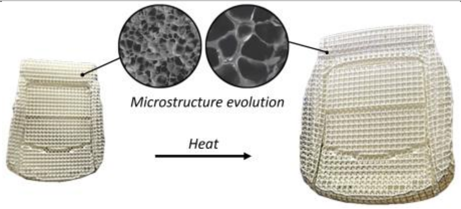	[92]
BPADA-GMA-BA (69:23:8)	Heating up to 60 C for shape transformation	Polymer actuator	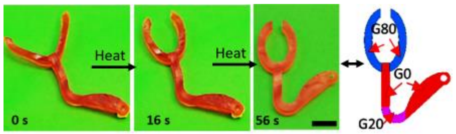	[7]
PEGDA-HEMA* (1:3) + CNT	Heating with electrical field for shape transformation	Polymer actuator	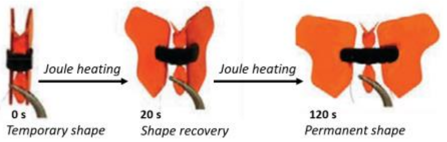	[89]

BDGE-PGBAPE-DC (3.4:0.69:0.66)	Heating with near-infrared (NIR) light for <u>shape</u> transformation	Heart patch	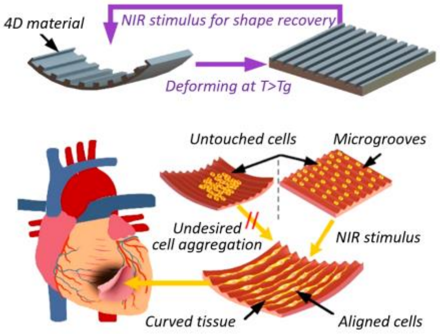	[88]
HAMA	Humidity and pH for <u>shape</u> transformation	Capillary and blood vessel tissue (with cells)	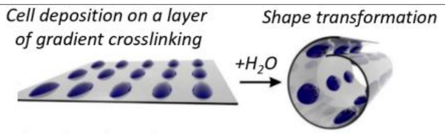	[84,90,91]
ChLCE *	Humidity for <u>color</u> transformation	Smart colored devices	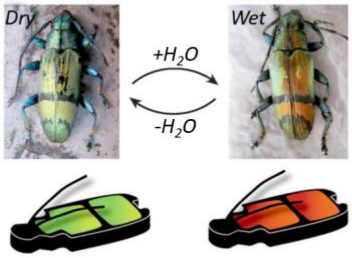	[87]

*** PHEMA: poly-hydroxy-ethyl-methacrylate; CNT: carbon nanotube; BDGE: bisphenol A di-glycidyl ether; PGBAPE: poly(propylene glycol) bis(2-aminopropyl) ether; DC: decylamine; ChLCE: (water-sensitive) cholesteric liquid crystal elastomer.**

6.2. Inks for Multi-Material Fabrication

Regarding the need for composite structures for biomanufacturing, recent efforts have been made to use advanced 3D printing to create complex, multi-component, micro-tissue models with a controlled cell-ECM-vasculature complex. DLP printing method benefits from a good speed and easy control over the mechanical properties of bioinks and a superior practical resolution down to ~ 10 µm compared to other methods. The X-Y resolution can approach around ~ 10 µm [2] (while ~ 1 µm for non-cellular inks), and the fabrication speed is typically between 0.5 and 10 mm/s (reaching 100 mm/s for non-cellular inks). Ultraviolet and infrared wavelengths are promisingly used for the rapid fabrication of tissue constructs by the DLP method. Applying other wavelengths, such as the green light, is less studied in the literature. Thus, DLP methods seem to be an ideal fit for the rapid fabrication of multi-material microtissues. In this direction, the main issues are the compatibility of different bioinks used to material exchange and how the interactions can impact their optical properties. A combination of standard inks introduced in **Table 2** may be utilized for multi-material DLP printing, provided all components can be dissolved in similar solvents. Table 3 provides information on the water solubility of typical monomers used in DLP ink formulations to check this condition. The tables would help to select a proper set of bioinks for multi-material fabrication.

7. Conclusions

This review covered (i) challenges in using different materials for multi-material printing, to be solved using microfluidic and dual-color photocrosslinking; (ii) challenges in improving resolution, to be solved by proper choice of inks, optical hardware, flashing photopolymerization, and others; and (iii) challenges in formulating inks and photoinitiator systems, to be addressed by light sheet technology and photoswitch systems. A detailed guideline was presented to help engineers in fabricating functional structures at improved resolutions. Light-material interactions such as refraction, scattering, and absorption phenomena were discussed for optimizing the fabrication process. The size of scattering particles and photon scattering were used to explain how to measure the quality of the DLP process. The roles of light wavelength, intensity, exposure time, and ink chemistry such as photoinitiator content, its molar absorptivity, and molecular structure of the ink monomer were explained on the curing depth or the effective resolution. Analysis of previous reports showed that decreasing the light wavelength improves the resolution in DLP platforms (see **Table 1**).

The photocrosslinking in DLP printers was modeled by theoretical optics to discover the correlation between the curing depth and the set of light parameters: exposure time, light intensity, and photoinitiator content. The phenomenological relationships revealed the nonlinear dependence of the photocuring depth on the process parameters and ink photochemistry. A photoinitiator threshold exists in the ink formulation, which allows achieving the highest curing depth in layer-by-layer printing [95]. Increasing light intensity beyond a conventional range increases fabrication costs, while improving the exposure time decreases printing speed, a hallmark of DLP printing. In layer-by-layer printing, the exposure time and the curing depth control the rate of fabrication. Redundant intensity, exposure time, and photoinitiator concentration raises light scattering, leading to overcuring and deteriorated resolution. Thus, engineers have to consider the light-matter interaction equations and fabrication parameters to control the printing quality.

We used experimental data to elucidate the role of monomer molecular weight on the resolution of DLP printing. In low molecular weight inks, acrylate groups were mainly attached as an end group to the backbone of molecular structure. With increasing the molecular weight, the relative density of acrylate groups reduced while light scattering was enhanced. By increasing molecular weight, the printing resolution was decreased. In high molecular weight inks, acrylate groups were attached as a side group, and the printing resolution was independent of the molecular weight as the density of acrylate groups remained constant by increasing the molecular weight; thus, no significant change was observed in obtained solution during DLP printing. General guidelines about ink material selection were given to achieve an improved resolution (**Figure 5**). At last, future trends in DLP printers for 4D and multi-material fabrication were discussed (**Table 4**). The discussions help material scientists and engineers select the proper combination of materials, photoinitiators, and optical parameters to improve 3D printing resolution in a DLP setup.

Author Contributions

Hossein G. Hosseinabadi: Conceptualization, Methodology, Writing- Original draft preparation, Formal analysis. **Daniel Nieto**: Investigation, Writing- Original draft preparation. **Ali Yousefinejad**: Data curation, Visualization. **Hoda Fattel**: Data curation, Visualization. **Leonid Ionov**: Supervision, Reviewing and Editing. **Amir K. Miri**: Supervision, Validation, Writing- Reviewing and Editing.

Acknowledgments

Hossein G. Hosseinabadi acknowledges the receipt of fellowship award funding by the Alexander von Humboldt Foundation during this research. **Amir K. Miri** acknowledges the receipt of a start-up fund from NJIT.

Conflict of Interests

The authors declare no competing financial interest.

References

[1] D. Ahn, L.M. Stevens, K. Zhou, Z.A. Page, Rapid High-Resolution Visible Light 3D Printing, ACS Cent. Sci. 6 (2020) 1555–1563. https://doi.org/10.1021/acscentsci.0c00929.

[2] A.K. Miri, D. Nieto, L. Iglesias, H. Goodarzi Hosseinabadi, S. Maharjan, G.U. Ruiz-Esparza, P. Khoshakhlagh, A. Manbachi, M.R. Dokmeci, S. Chen, S.R. Shin, Y.S. Zhang, A. Khademhosseini, Microfluidics-Enabled Multimaterial Maskless Stereolithographic Bioprinting, Adv. Mater. 30 (2018) 1–9. https://doi.org/10.1002/adma.201800242.

[3] Y. Lu, G. Mapili, G. Suhali, S. Chen, K. Roy, A digital micro-mirror device-based system for the microfabrication of complex, spatially patterned tissue engineering scaffolds, J. Biomed. Mater. Res. - Part A. 77 (2006) 396–405. https://doi.org/10.1002/jbm.a.30601.

[4] H. Goodarzi Hosseinabadi, E. Dogan, A.K. Miri, L. Ionov, Digital Light Processing Bioprinting Advances for Microtissue Models, ACS Biomater. Sci. Eng. 8 (2022) 1381. https://doi.org/10.1021/acsbiomaterials.1c01509.

[5] Absolute Reports® - Market research Reports and Industry Analysis Reports, (n.d.). https://www.absolutereports.com/ (accessed February 14, 2022).

[6] A. Bhusal, E. Dogan, H.-A. Nguyen, O. Labutina, D. Nieto, A.K. Miri, Multi-material digital light processing bioprinting of hydrogel-based microfluidic chips, Biofabrication. 14 (2022) 014103. https://doi.org/10.1088/1758-5090/ac2d78.

[7] X. Kuang, J. Wu, K. Chen, Z. Zhao, Z. Ding, F. Hu, D. Fang, H.J. Qi, Grayscale digital light processing 3D printing for

highly functionally graded materials, Sci. Adv. 5 (2019). https://doi.org/10.1126/SCIADV.AAV5790.

[8] E. Dogan, A. Bhusal, B. Cecen, A.K. Miri, 3D Printing metamaterials towards tissue engineering, Appl. Mater. Today. 20 (2020). https://doi.org/10.1016/j.apmt.2020.100752.

[9] J.E. Shaw, R.A. Sicree, P.Z. Zimmet, Global estimates of the prevalence of diabetes for 2010 and 2030, Diabetes Res. Clin. Pract. 87 (2010) 4–14. https://doi.org/10.1016/j.diabres.2009.10.007.

[10] A.M.J. Shapiro, M. Pokrywczynska, C. Ricordi, Clinical pancreatic islet transplantation, Nat. Rev. Endocrinol. 13 (2017) 268–277. https://doi.org/10.1038/nrendo.2016.178.

[11] A. Bruni, B. Gala-Lopez, A.R. Pepper, N.S. Abualhassan, A.M. James Shapiro, Islet cell transplantation for the treatment of type 1 diabetes: Recent advances and future challenges, Diabetes, Metab. Syndr. Obes. Targets Ther. 7 (2014) 211–223. https://doi.org/10.2147/DMSO.S50789.

[12] A.S. Theus, L. Ning, B. Hwang, C. Gil, S. Chen, A. Wombwell, R. Mehta, V. Serpooshan, Bioprintability: Physiomechanical and biological requirements of materials for 3d bioprinting processes, Polymers (Basel). 12 (2020) 1–19. https://doi.org/10.3390/polym12102262.

[13] O. Nakamura, S. Kawata, S. Maruo, Three-dimensional microfabrication with two-photon-absorbed photopolymerization, Opt. Lett. Vol. 22, Issue 2, Pp. 132-134. 22 (1997) 132–134. https://doi.org/10.1364/OL.22.000132.

[14] H.G. Hosseinabadi, R. Bagheri, L. Avila Gray, V. Altstädt, K. Drechsler, Plasticity in polymeric honeycombs made by photo-polymerization and nozzle based 3D-printing, Polym. Test. 63 (2017) 163–167. https://doi.org/10.1016/j.polymertesting.2017.08.008.

[15] H. Goodarzi Hosseinabadi, R. Bagheri, V. Altstädt, Shear band propagation in honeycombs: numerical and experimental, Rapid Prototyp. J. 24 (2018). https://doi.org/10.1108/RPJ-06-2016-0098.

[16] Z. Gu, J. Fu, H. Lin, Y. He, Development of 3D bioprinting: From printing methods to biomedical applications, Asian J. Pharm. Sci. 15 (2020) 529–557. https://doi.org/10.1016/j.ajps.2019.11.003.

[17] K. Kowsari, W. Lee, S.S. Yoo, N.X. Fang, Scalable visible light 3D printing and bioprinting using an organic light-emitting diode microdisplay, IScience. 24 (2021) 103372. https://doi.org/10.1016/j.isci.2021.103372.

[18] H.H. Hwang, W. Zhu, G. Victorine, N. Lawrence, S. Chen, 3D-Printing of Functional Biomedical Microdevices via Light- and Extrusion-Based Approaches, Small Methods. 2 (2018) 1–18. https://doi.org/10.1002/smtd.201700277.

[19] B. Zhang, W. Wang, X. Gui, P. Song, H. Lei, Z. Li, C. Zhou, Y. Fan, X. Zhang, 3D printing of customized key biomaterials genomics for bone regeneration, Appl. Mater. Today. 26 (2022) 101346. https://doi.org/10.1016/j.apmt.2021.101346.

[20] P. Song, M. Li, B. Zhang, X. Gui, Y. Han, L. Wang, W. Zhou, L. Guo, Z. Zhang, Z. Li, C. Zhou, Y. Fan, X. Zhang, DLP fabricating of precision GelMA/HAp porous composite scaffold for bone tissue engineering application, Compos. Part B Eng. 244 (2022) 110163. https://doi.org/10.1016/J.COMPOSITESB.2022.110163.

[21] A. Mazzocchi, S. Soker, A. Skardal, 3D bioprinting for high-throughput screening: Drug screening, disease modeling, and precision medicine applications, Appl. Phys. Rev. 6 (2019). https://doi.org/10.1063/1.5056188.

[22] S. Samavedi, N. Joy, 3D printing for the development of in vitro cancer models, Curr. Opin. Biomed. Eng. 2 (2017) 35–42. https://doi.org/10.1016/j.cobme.2017.06.003.

[23] A. Blaeser, D.F. Duarte Campos, H. Fischer, 3D bioprinting of cell-laden hydrogels for advanced tissue engineering, Curr. Opin. Biomed. Eng. 2 (2017) 58–66. https://doi.org/10.1016/j.cobme.2017.04.003.

[24] S. Samavedi, N. Joy, 3D printing for the development of in vitro cancer models, Curr. Opin. Biomed. Eng. 2 (2017) 35–42. https://doi.org/10.1016/j.cobme.2017.06.003.

[25] A.K. Miri, E. Mostafavi, D. Khorsandi, S.-K. Huc, M. Malpica, A. Kkhademhosseini, 12, Khademhosseini, Bioprinters for organs-on-chips, Biofabrication,. (2019) 0–23. https://iopscience.iop.org/article/10.1088/2053-1583/abe778.

[26] A.K. Miri, A. Khalilpour, B. Cecen, S. Maharjan, S.R. Shin, A. Khademhosseini, Multiscale bioprinting of vascularized models, Biomaterials. 198 (2019) 204–216. https://doi.org/10.1016/j.biomaterials.2018.08.006.

[27] F.P.W. Melchels, J. Feijen, D.W. Grijpma, A review on stereolithography and its applications in biomedical engineering, Biomaterials. 31 (2010) 6121–6130. https://doi.org/10.1016/j.biomaterials.2010.04.050.

[28] C.W. Hull, C. Arcadia, United States Patent (19) Hull (54) (75) (73) 21) 22 (51) 52) (58) (56) APPARATUS FOR PRODUCTION OF THREE-DMENSONAL OBJECTS BY STEREO THOGRAPHY, 1984.

[29] A. Blaeser, D.F. Duarte Campos, H. Fischer, 3D bioprinting of cell-laden hydrogels for advanced tissue engineering, Curr. Opin. Biomed. Eng. 2 (2017) 58–66. https://doi.org/10.1016/j.cobme.2017.04.003.

[30] A. V. Nielsen, M.J. Beauchamp, G.P. Nordin, A.T. Woolley, 3D Printed Microfluidics, Annu. Rev. Anal. Chem. 13 (2020) 45–65. https://doi.org/10.1146/annurev-anchem-091619-102649.

[31] B. Zhang, X. Gui, P. Song, X. Xu, L. Guo, Y. Han, L. Wang, C. Zhou, Y. Fan, X. Zhang, Three-Dimensional Printing of Large-Scale, High-Resolution Bioceramics with Micronano Inner Porosity and Customized Surface Characterization Design for Bone Regeneration, ACS Appl. Mater. Interfaces. 14 (2022) 8804–8815. https://doi.org/10.1021/ACSAMI.1C22868/SUPPL_FILE/AM1C22868_SI_005.PDF.

[32] C. von Horst, www.plastinate.com, HC Biovision, Ger. (2020). www.plastinate.com (accessed October 7, 2022).

[33] S. You, J. Guan, J. Alido, H.H. Hwang, R. Yu, L. Kwe, H. Su, S. Chen, Mitigating scattering effects in light-based three-dimensional printing using machine learning, J. Manuf. Sci. Eng. Trans. ASME. 142 (2020) 1–10. https://doi.org/10.1115/1.4046986.

[34] S. Catros, J.C. Fricain, B. Guillotin, B. Pippenger, R. Bareille, M. Remy, E. Lebraud, B. Desbat, J. Amédée, F. Guillemot, Laser-assisted bioprinting for creating on-demand patterns of human osteoprogenitor cells and nano-hydroxyapatite, Biofabrication. 3 (2011). https://doi.org/10.1088/1758-5082/3/2/025001.

[35] M. Farsari, B.N. Chichkov, Materials processing: Two-photon fabrication, Nat. Photonics. 3 (2009) 450–452. https://doi.org/10.1038/nphoton.2009.131.

[36] S. You, J. Li, W. Zhu, C. Yu, D. Mei, S. Chen, Nanoscale 3D printing of hydrogels for cellular tissue engineering, J. Mater. Chem. B. 6 (2018) 2187–2197. https://doi.org/10.1039/c8tb00301g.

[37] D. Wu, Z. Zhao, Q. Zhang, H.J. Qi, D. Fang, Mechanics of shape distortion of DLP 3D printed structures during UV post-curing, 2019. https://doi.org/10.1039/c9sm00725c.

[38] N.N. Kumbhar, A. V. Mulay, Post Processing Methods used to Improve Surface Finish of Products which are Manufactured by Additive Manufacturing Technologies: A Review, J. Inst. Eng. Ser. C. 99 (2018) 481–487. https://doi.org/10.1007/s40032-016-0340-z.

[39] J. Zhang, Q. Hu, S. Wang, J. Tao, M. Gou, Digital light processing based three-dimensional printing for medical applications, Int. J. Bioprinting. 6 (2020) 12–27. https://doi.org/10.18063/ijb.v6i1.242.

[40] W. Zhu, X. Ma, M. Gou, D. Mei, K. Zhang, S. Chen, 3D printing of functional biomaterials for tissue engineering, Curr. Opin. Biotechnol. 40 (2016) 103–112. https://doi.org/10.1016/j.copbio.2016.03.014.

[41] X. Ma, J. Liu, W. Zhu, M. Tang, N. Lawrence, C. Yu, M. Gou, S. Chen, 3D bioprinting of functional tissue models for personalized drug screening and in vitro disease modeling, Adv. Drug Deliv. Rev. 132 (2018) 235–251. https://doi.org/10.1016/j.addr.2018.06.011.

[42] B. Grigoryan, S.J. Paulsen, D.C. Corbett, D.W. Sazer, C.L. Fortin, A.J. Zaita, P.T. Greenfield, N.J. Calafat, J.P. Gounley, A.H. Ta, F. Johansson, A. Randles, J.E. Rosenkrantz, J.D. Louis-Rosenberg, P.A. Galie, K.R. Stevens, J.S. Miller, Multivascular networks and functional intravascular topologies within biocompatible hydrogels, Science (80-.). 364 (2019) 458–464. https://doi.org/10.1126/SCIENCE.AAV9750.

[43] X. Ma, X. Qu, W. Zhu, Y.-S.S. Li, S. Yuan, H. Zhang, J. Liu, P. Wang, C.S.E. Lai, F. Zanella, G.-S.S. Feng, F. Sheikh, S. Chien, S. Chen, Deterministically patterned biomimetic human iPSC-derived hepatic model via rapid 3D bioprinting, Proc. Natl. Acad. Sci. U. S. A. 113 (2016) 2206–2211. https://doi.org/10.1073/pnas.1524510113.

[44] K.S. Lim, R. Levato, P.F. Costa, M.D. Castilho, C.R. Alcala-Orozco, K.M.A. Van Dorenmalen, F.P.W. Melchels, D. Gawlitta, G.J. Hooper, J. Malda, T.B.F. Woodfield, Bio-resin for high resolution lithography-based biofabrication of complex cell-laden constructs, Biofabrication. 10 (2018). https://doi.org/10.1088/1758-5090/aac00c.

[45] X. Ma, S. Dewan, J. Liu, M. Tang, K.L. Miller, C. Yu, N. Lawrence, A.D. McCulloch, S. Chen, 3D printed micro-scale force gauge arrays to improve human cardiac tissue maturation and enable high throughput drug testing, Acta Biomater. 95 (2019) 319–327. https://doi.org/10.1016/j.actbio.2018.12.026.

[46] J. Liu, J. He, J. Liu, X. Ma, Q. Chen, N. Lawrence, W. Zhu, Y. Xu, S. Chen, Rapid 3D bioprinting of in vitro cardiac tissue models using human embryonic stem cell-derived cardiomyocytes, Bioprinting. 13 (2019) e00040.

https://doi.org/10.1016/j.bprint.2019.e00040.

[47] J. Koffler, W. Zhu, X. Qu, O. Platoshyn, J.N. Dulin, J. Brock, L. Graham, P. Lu, J. Sakamoto, M. Marsala, S. Chen, M.H. Tuszynski, Biomimetic 3D-printed scaffolds for spinal cord injury repair, Nat. Med. 25 (2019) 263–269. https://doi.org/10.1038/s41591-018-0296-z.

[48] C. Höhne, M. Schmitter, 3D Printed Teeth for the Preclinical Education of Dental Students, J. Dent. Educ. 83 (2019) 1100–1106. https://doi.org/10.21815/jde.019.103.

[49] W. Zhu, K.R. Tringale, S.A. Woller, S. You, S. Johnson, H. Shen, J. Schimelman, M. Whitney, J. Steinauer, W. Xu, T.L. Yaksh, Q.T. Nguyen, S. Chen, Rapid continuous 3D printing of customizable peripheral nerve guidance conduits, Mater. Today. 21 (2018) 951–959. https://doi.org/10.1016/j.mattod.2018.04.001.

[50] R.B. Osman, A.J. van der Veen, D. Huiberts, D. Wismeijer, N. Alharbi, 3D-printing zirconia implants; a dream or a reality? An in-vitro study evaluating the dimensional accuracy, surface topography and mechanical properties of printed zirconia implant and discs, J. Mech. Behav. Biomed. Mater. 75 (2017) 521–528. https://doi.org/10.1016/j.jmbbm.2017.08.018.

[51] Y. Chen, J. Zhang, X. Liu, S. Wang, J. Tao, Y. Huang, W. Wu, Y. Li, K. Zhou, X. Wei, S. Chen, X. Li, X. Xu, L. Cardon, Z. Qian, M. Gou, Noninvasive in vivo 3D bioprinting, Sci. Adv. 6 (2020) 1–11. https://doi.org/10.1126/sciadv.aba7406.

[52] Z. Wang, R. Abdulla, B. Parker, R. Samanipour, S. Ghosh, K. Kim, A simple and high-resolution stereolithography-based 3D bioprinting system using visible light crosslinkable bioinks, Biofabrication. 7 (2015). https://doi.org/10.1088/1758-5090/7/4/045009.

[53] B. Grigoryan, D.W. Sazer, A. Avila, J.L. Albritton, A. Padhye, A.H. Ta, P.T. Greenfield, D.L. Gibbons, J.S. Miller, Development, characterization, and applications of multi-material stereolithography bioprinting, Sci. Rep. 11 (2021) 1–13. https://doi.org/10.1038/s41598-021-82102-w.

[54] S. You, P. Wang, J. Schimelman, H.H. Hwang, S. Chen, High-fidelity 3D printing using flashing photopolymerization, Addit. Manuf. 30 (2019) 100834. https://doi.org/10.1016/j.addma.2019.100834.

[55] D. Xue, Y. Wang, J. Zhang, D. Mei, Y. Wang, S. Chen, Projection-Based 3D Printing of Cell Patterning Scaffolds with Multiscale Channels, ACS Appl. Mater. Interfaces. 10 (2018) 19428–19435. https://doi.org/10.1021/acsami.8b03867.

[56] Z. Zhong, X. Deng, P. Wang, C. Yu, W. Kiratitanaporn, X. Wu, J. Schimelman, M. Tang, A. Balayan, E. Yao, J. Tian, L. Chen, K. Zhang, S. Chen, Rapid bioprinting of conjunctival stem cell micro-constructs for subconjunctival ocular injection, Biomaterials. 267 (2021) 120462. https://doi.org/10.1016/j.biomaterials.2020.120462.

[57] M. Regehly, Y. Garmshausen, M. Reuter, N.F. König, E. Israel, D.P. Kelly, C.Y. Chou, K. Koch, B. Asfari, S. Hecht, Xolography for linear volumetric 3D printing, Nature. 588 (2020) 620–624. https://doi.org/10.1038/s41586-020-3029-7.

[58] K.S. Lim, R. Levato, P.F. Costa, M.D. Castilho, C.R. Alcala-Orozco, K.M.A. van Dorenmalen, F.P.W. Melchels, D. Gawlitta, G.J. Hooper, J. Malda, T.B.F. Woodfield, Bio-resin for high resolution lithography-based biofabrication of complex cell laden constructs, Biofabrication. 10 (2018). https://iopscience.iop.org/article/10.1088/2053-1583/abe778.

[59] K. Mizuguchi, Y. Nagano, H. Nishiyama, H. Onoe, M. Terakawa, Multiphoton photoreduction for dual-wavelength-light-driven shrinkage and actuation in hydrogel, Opt. Mater. Express. 10 (2020) 1931. https://doi.org/10.1364/ome.399874.

[60] Z. Wang, Development of a visible light stereolithography-based bioprinting system for tissue engineering, Tianjin University, 2016.

[61] B. Grigoryan, S.J. Paulsen, D.C. Corbett, D.W. Sazer, C.L. Fortin, A.J. Zaita, P.T. Greenfield, N.J. Calafat, J.P. Gounley, A.H. Ta, F. Johansson, A. Randles, J.E. Rosenkrantz, J.D. Louis-Rosenberg, P.A. Galie, K.R. Stevens, J.S. Miller, Multivascular networks and functional intravascular topologies within biocompatible hydrogels, (n.d.). http://science.sciencemag.org/ (accessed August 19, 2021).

[62] W. Zhu, X. Qu, J. Zhu, X. Ma, S. Patel, J. Liu, P. Wang, C.S.E. Lai, M. Gou, Y. Xu, K. Zhang, S. Chen, Direct 3D bioprinting of prevascularized tissue constructs with complex microarchitecture, Biomaterials. 124 (2017) 106–115. https://doi.org/10.1016/j.biomaterials.2017.01.042.

[63] P. Wang, X. Li, W. Zhu, Z. Zhong, A. Moran, W. Wang, K. Zhang, S. Chen, 3D bioprinting of hydrogels for retina cell culturing, Bioprinting. 12 (2018) 1–6. https://doi.org/10.1016/j.bprint.2018.e00029.

[64] J. Liu, K. Miller, X. Ma, S. Dewan, N. Lawrence, G. Whang, P. Chung, A.D. McCulloch, S. Chen, Direct 3D bioprinting of cardiac micro-tissues mimicking native myocardium, Biomaterials. 256 (2020). https://doi.org/10.1016/j.biomaterials.2020.120204.

[65] A. Thomas, I. Orellano, T. Lam, B. Noichl, M.A. Geiger, A.K. Amler, A.E. Kreuder, C. Palmer, G. Duda, R. Lauster, L. Kloke, Vascular bioprinting with enzymatically degradable bioinks via multi-material projection-based stereolithography, Acta Biomater. 117 (2020) 121–132. https://doi.org/10.1016/j.actbio.2020.09.033.

[66] T. Lam, T. Dehne, J.P. Krüger, S. Hondke, M. Endres, A. Thomas, R. Lauster, M. Sittinger, L. Kloke, Photopolymerizable gelatin and hyaluronic acid for stereolithographic 3D bioprinting of tissue-engineered cartilage, J. Biomed. Mater. Res. B. Appl. Biomater. 107 (2019) 2649–2657. https://doi.org/10.1002/JBM.B.34354.

[67] W. Li, M. Wang, L.S. Mille, J.A. Robledo Lara, V. Huerta, T. Uribe Velázquez, F. Cheng, H. Li, J. Gong, T. Ching, C.A. Murphy, A. Lesha, S. Hassan, T.B.F. Woodfield, K.S. Lim, Y.S. Zhang, A Smartphone-Enabled Portable Digital Light Processing 3D Printer, Adv. Mater. (2021) 2102153. https://doi.org/10.1002/ADMA.202102153.

[68] Y. Yang, Y. Zhou, X. Lin, Q. Yang, G. Yang, Printability of External and Internal Structures Based on Digital Light Processing 3D Printing Technique, Pharmaceutics. 12 (2020) 207.

[69] S. Johnsen, E.A. Widder, The physical basis of transparency in biological tissue: ultrastructure and the minimization of light scattering, J. Theor. Biol. 199 (1999) 181–198. https://doi.org/10.1006/JTBI.1999.0948.

[70] D. Watson, N. Hagen, J. Diver, P. Marchand, M. Chachisvilis, Elastic Light Scattering from Single Cells: Orientational Dynamics in Optical Trap, Biophys. J. 87 (2004) 1298. https://doi.org/10.1529/BIOPHYSJ.104.042135.

[71] S. Zissi, A. Bertsch, J.Y. Jézéquel, S. Corbel, D.J. Lougnot, J.C. André, Stereolithography and microtechniques, Microsyst. Technol. 2 (1995) 97–102. https://doi.org/10.1007/BF02739538.

[72] K. Khairu, I. Raman, M.A.S. Mohamed, M. Ibrahim, M.S. Wahab, Parameter optimerization for photo polymerization of microstereolithography, Adv. Mater. Res. 626 (2013) 420–424. https://doi.org/10.4028/www.scientific.net/AMR.626.420.

[73] S. Kumar, J. Aaron, K. Sokolov, Directional conjugation of antibodies tonanoparticles for synthesis of multiplexed opticalcontrast agents with both delivery and targetingmoieties, (2008) 314.

[74] E.G. Wrigglesworth, J.H. Johnston, Mie theory and the dichroic effect for spherical gold nanoparticles: an experimental approach, Nanoscale Adv. 3 (2021) 3530–3536. https://doi.org/10.1039/D1NA00148E.

[75] M. Chen, M. Zhong, J.A. Johnson, Light-Controlled Radical Polymerization: Mechanisms, Methods, and Applications, Chem. Rev. 116 (2016) 10167–10211. https://doi.org/10.1021/ACS.CHEMREV.5B00671.

[76] J.H. Lee, R.K. Prud'homme, I.A. Aksay, Cure depth in photopolymerization: Experiments and theory, J. Mater. Res. 16 (2001) 3536–3544. https://doi.org/10.1557/JMR.2001.0485.

[77] Y. Shen, H. Tang, X. Huang, R. Hang, X. Zhang, Y. Wang, X. Yao, DLP printing photocurable chitosan to build bio-constructs for tissue engineering, Carbohydr. Polym. 235 (2020) 115970. https://doi.org/10.1016/j.carbpol.2020.115970.

[78] Y. Shen, H. Tang, X. Huang, R. Hang, X. Zhang, Y. Wang, X. Yao, DLP printing photocurable chitosan to build bio-constructs for tissue engineering, Carbohydr. Polym. 235 (2020) 115970. https://doi.org/10.1016/j.carbpol.2020.115970.

[79] G. Melilli, I. Carmagnola, C. Tonda-Turo, F. Pirri, G. Ciardelli, M. Sangermano, M. Hakkarainen, A. Chiappone, DLP 3D Printing Meets Lignocellulosic Biopolymers: Carboxymethyl Cellulose Inks for 3D Biocompatible Hydrogels, (n.d.). https://doi.org/10.3390/polym12081655.

[80] S.H. Kim, Y.K. Yeon, J.M. Lee, J.R. Chao, Y.J. Lee, Y.B. Seo, M.T. Sultan, O.J. Lee, J.S. Lee, S. Il Yoon, I.S. Hong, G. Khang, S.J. Lee, J.J. Yoo, C.H. Park, Precisely printable and biocompatible silk fibroin bioink for digital light processing 3D printing, Nat. Commun. 9 (2018) 1–14. https://doi.org/10.1038/s41467-018-03759-y.

[81] H. Kwak, S. Shin, H. Lee, J. Hyun, Formation of a keratin layer with silk fibroin-polyethylene glycol composite hydrogel fabricated by digital light processing 3D printing, J. Ind. Eng. Chem. 72 (2019) 232–240. https://doi.org/10.1016/j.jiec.2018.12.023.

[82] U. Shaukat, E. Rossegger, S. Schlögl, Thiol–acrylate based vitrimers: From their structure–property relationship to the additive manufacturing of self-healable soft active devices, Polymer (Guildf). 231 (2021) 29–34. https://doi.org/10.1016/j.polymer.2021.124110.

[83] J. Su, Thiol-Mediated Chemoselective Strategies for In Situ Formation of Hydrogels, Gels 2018, Vol. 4, Page 72. 4 (2018) 72. https://doi.org/10.3390/GELS4030072.

[84] I. Apsite, A. Biswas, Y. Li, L. Ionov, Microfabrication Using Shape-Transforming Soft Materials, Adv. Funct. Mater. 30 (2020). https://doi.org/10.1002/adfm.201908028.

[85] G. Zhu, Y. Hou, J. Xu, N. Zhao, Reprintable Polymers for Digital Light Processing 3D Printing, Adv. Funct. Mater. 31 (2021). https://doi.org/10.1002/ADFM.202007173.

[86] T. Van Manen, S. Janbaz, K. Jansen, A.A. Zadpoor, 4D printing of reconfigurable metamaterials and devices, (n.d.). https://doi.org/10.1038/s43246-021-00165-8.

[87] J.A.H.P.H.P. Sol, L.G. Smits, A.P.H.J.H.J. Schenning, M.G. Debije, J.A.H.P.H.P. Sol, L.G. Smits, A.P.H.J.H.J. Schenning, M.G. Debije, Direct Ink Writing of 4D Structural Colors, Adv. Funct. Mater. (2022). https://doi.org/10.1002/ADFM.202201766.

[88] Y. Wang, H. Cui, Y. Wang, C. Xu, T.J. Esworthy, S.Y. Hann, M. Boehm, Y.L. Shen, D. Mei, L.G. Zhang, 4D Printed Cardiac Construct with Aligned Myofibers and Adjustable Curvature for Myocardial Regeneration, ACS Appl. Mater. Interfaces. 13 (2021) 12746–12758. https://doi.org/10.1021/acsami.0c17610.

[89] A. Cortés, A. Cosola, M. Sangermano, M. Campo, S.G. Prolongo, C. Fabrizio Pirri, A. Jiménez-Suárez, A. Chiappone, A. Cortés, M. Campo, S. González, A. Jiménez-Suárez, A. Cosola, M. Sangermano, C.F. Pirri, A. Chiappone, DLP 4D-Printing of Remotely, Modularly, and Selectively Controllable Shape Memory Polymer Nanocomposites Embedding Carbon Nanotubes, Adv. Funct. Mater. 31 (2021) 2106774. https://doi.org/10.1002/ADFM.202106774.

[90] I. Apsite, S. Salehi, L. Ionov, Materials for Smart Soft Actuator Systems, Chem. Rev. 122 (2022) 1349–1415. https://doi.org/10.1021/acs.chemrev.1c00453.

[91] A. Kirillova, R. Maxson, G. Stoychev, C.T. Gomillion, L. Ionov, 4D Biofabrication Using Shape-Morphing Hydrogels, Adv. Mater. 29 (2017) 1–8. https://doi.org/10.1002/adma.201703443.

[92] K. Sertoglu, Desktop Metal unveils new expandable foam 3D printing material, FreeFoam - 3D Printing Industry, (2022). https://3dprintingindustry.com/news/desktop-metal-unveils-new-expandable-foam-3d-printing-material-freefoam-211265/ (accessed July 6, 2022).

[93] M.A. Gerkman, R.S.L. Gibson, J. Calbo, Y. Shi, M.J. Fuchter, G.G.D. Han, Arylazopyrazoles for Long-Term Thermal Energy Storage and Optically Triggered Heat Release below 0 °c, J. Am. Chem. Soc. 142 (2020) 8688–8695. https://doi.org/10.1021/jacs.0c00374.

[94] N.A. Simeth, S. Crespi, M. Fagnoni, B. König, Tuning the Thermal Isomerization of Phenylazoindole Photoswitches from Days to Nanoseconds, J. Am. Chem. Soc. 140 (2018) 2940–2946. https://doi.org/10.1021/jacs.7b12871.

[95] P.F. Jacobs, Rapid Prototyping & Manufacturing, (1992) 1–369.

[96] G. Merkininkaitė, D. Gailevičius, S. Šakirzanovas, L. Jonušauskas, Polymers for Regenerative Medicine Structures Made via Multiphoton 3D Lithography, Int. J. Polym. Sci. 2019 (2019). https://doi.org/10.1155/2019/3403548.

[97] G. Keifer, F. Effenberger, Odian Principles of Polymerization, 1967.

Supplementary Material

DLP printing mechanism comprises single photon absorption, which means that the photopolymerization process in DLP platforms initiates from a linear single photon absorption [96]. In this case, the energy of the UV photon, E_p, is equal to or superior to the ink material bandgap E_g. The law that governs this process is:

$$E_p = hv = h\,\frac{c}{\lambda} \qquad \text{(S1)}$$

This means high-energy photons and short wavelengths (~ 365 nm) are preferred to initiate DLP printing. One photon absorption with $E_p > E_g$ promotes the electron to travel from the valence band to the conduction band. This process modifies the chemical bond prompting the polymerization process, which ultimately becomes responsible for crosslinking the ink material. DLP platforms mostly use a noncoherent light source. As the light intensity rises, usually by using coherent laser sources, nonlinear absorption can take place. The UV (λ_{UV}) photosensitive ink material can also be photopolymerized by infrared (IR) wavelength of nearly double wavelength (λ_{IR}=2 λ_{UV}) [13]. Each initiator system which usually absorbs a UV photon (395 nm), can absorb two near IR photons (790 nm) simultaneously and provide a free radical when the spatial density of the near IR photons is strong enough. The resultant radicals then will cut the double bonds of carbons in the acrylic groups and successively create new radicals to proceed with the photopolymerization reaction [13].

It is then required to precisely determining the depth of curing (layer height), the printing speed, and the dimensions of the final cured structure. A standard design equation defines the thickness of a light-cured material in stereolithography by:

$$C_d = D_p \ln\left(\frac{E_{max}}{E_c}\right) \qquad \text{(S2)}$$

where C_d is the depth of curing (μm), D_p is the depth of light penetration (μm), E_{max} is the maximum irradiation of light per area (mJ/cm^2) at the vat surface, and E_c is the threshold value of energy required for gelation of the liquid ink (mJ/cm^2). As E_{max} approaches E_c, the gelation point is reached, the monomers are polymerized, and the ink solidifies [67,76,95].

Following Jacobs [95] who solved kinetics equations for laser-based stereolithography and ignored diffraction and scattering, here we explain the same theoretical model for photocuring in a DLP printer. To this aim, we furnish those equations based on the light intensity and the exposure time, which technically can be programmed in DLP software. We explain how the ink chemistry, such as photoinitiator concentration and extinction coefficient, and the processing parameters, such as intensity and exposure time, affect the curing depth. The curing depth is an important parameter that affects the designed speed of 3D printing. The kinetics equations for photopolymerization reaction state that [97]:

$$\begin{cases} -\frac{d[M]}{dt} \approx R_p \\ R_p = k_p[M][M^{\cdot}] \end{cases} \tag{S3}$$

where R_p is the polymerization rate, [M] is the monomer concentration, $[M^{\cdot}]$ is the radical chain concentration, and k_p is the kinetic rate constant for propagation. Considering the intensity decay at the mirror edges, we use a simplified assumption that each mirror has a Gaussian distribution of intensity reflection. Assuming steady-state conditions (where the rate of initiation of free radicals, R_i, equals their termination by polymerization), one obtains [95]:

$$[M^{\cdot}] = \sqrt{\frac{R_i}{2k_{tr}}} \tag{S4}$$

where k_{tr} is the kinetic rate constant for termination reaction. For the photoinitiator, the following equation governs the initiation rate, R_i, and the photonic flux or, equivalently the incident light intensity at depth z, I_z [97].

$$R_i = 2\phi\epsilon_\lambda[PI]I_z \tag{S5}$$

Here, ϕ is the quantum yield of the photoinitiator, ϵ_λ is the molar extinction coefficient (monophotonic absorption) of the photoinitiator at wavelength λ, and [PI] is the molar concentration of the photoinitiator. Practically, most of the incident light passes straight through the ink, and photoinitiators absorb few amounts of photons. The light is not absorbed homogeneously throughout the ink layer. Beer-Lambert law states that light intensity decreases exponentially with the penetration depth:

$$I_z = I_0 e^{-z\epsilon_\lambda[PI]} \tag{S6}$$

where, I_0 is the maximum intensity of the incident light at the vat surface. Substituting **Eq. S4-S6** and into **Eq. S3** allows to obtain:

$$-\frac{d[M]}{dt} \approx R_p = k_p[M]\sqrt{\frac{\phi\epsilon_\lambda[PI]I_0 e^{-z\epsilon_\lambda[PI]}}{k_{tr}}} \tag{S7}$$

Separating variables and integrating the equation by assuming time independency of the constants gives:

$$\frac{\alpha^2}{I_0 t^2} = [PI]e^{-z\epsilon_\lambda[PI]} \tag{S8}$$

where $\alpha^2 = \frac{k_{tr}\ln\left(\frac{[M]_0}{[M]}\right)^2}{k_p^2\epsilon\phi}$ denotes to the photochemical characteristics of the ink formulation, and the term $\frac{[M]_0}{[M]}$ is simply the degree of polymerization which corresponds to the extent of polymerization, p, by $\frac{[M]_0}{[M]} = \frac{1}{1-p}$. At the gelation point, $p = p_c$ which is the critical threshold for converting the ink into gel and thus it can be used to calculate the limit of the curing depth, z_c[95]. Solving **Eq. S8** for z_c gives:

$$z_c = \frac{1}{[PI]\epsilon}\ln\left(\frac{[PI]I_0t^2}{\alpha^2}\right) \tag{S9}$$

Considering $\alpha^2 = 4.2 \times 10^{-6}\ \mathrm{Ms^{0.5}cm^{0.5}}$ for the monomer and $\epsilon = 23'000\ \mathrm{M^{-1}cm^{-1}}$ for the photoinitiator at 325 nm from Lee et al. [76], 3D curves and relevant 2D contour plots shown in **Figure 4** are obtained. **Eq. S9** clearly shows the relation of curing depth to the photoinitiator concentration, its molar extinction, the light intensity, and the exposure time as independent processing parameters during DLP printing. To calculate the optimal cure depth, we set zero the derivative of z_c with respect to [PI]:

$$\frac{dz_c}{d[PI]} = -\frac{1}{[PI]^2\epsilon}\ln\left(\frac{[PI]I_0t^2}{\alpha^2}\right) + \frac{1}{[PI]^2\epsilon} = 0 \longrightarrow [PI]_{optimal} = \frac{2.718\alpha^2}{I_0t^2} \tag{S10}$$

and the maximum curing depth at the threshold [PI] is achieved as a function of light intensity and exposure time by $z_c|_{[PI]_{optimal}} = \frac{I_0t^2}{2.718\epsilon\alpha^2}$. The maximum energy exposure per unit area, denoted by E_{max} in stereolithography literature, can be obtained by [95]:

$$E_{max} = \left(\frac{hcN_{av}}{\lambda}\right)I_0t \tag{S11}$$

N_{av} is Avogadro number. When **Eq. S11** is replaced in **Eq. S9**, we have:

$$z_c = \frac{2}{[PI]\epsilon}ln\left(\frac{\sqrt{[PI]}E_{max}}{\alpha\beta}\right) \tag{S12}$$

where $\beta = \frac{hcN_{av}\sqrt{I_0}}{\lambda}$ is a constant incorporating DLP processing and optical parameters while α is a previously introduced constant containing only the photochemical parameters of the ink. With making correspondence between this equation and the empirical standard equation (**Eq. S2),** and recognizing C_d as z_c, an obvious logarithmic dependence of the cure depth to the maximum energy dosage per area, E_{max}, is observed. As summarized in **Eq. S13**, the penetration depth D_p is inversely dependent on the photoinitiator concentration and extinction coefficient. The empirically derived E_c parameter is inversely dependent on the photoinitiator concentration to the one-half power as well as both the processing/optics and the photochemical characteristics of the ink formulation:

$$D_p = \frac{2}{[PI]\epsilon},\ E_c = \frac{\alpha\beta}{\sqrt{[PI]}} \tag{S13}$$

Supplementary Data

Table S1. Measured values for resolution in crosslinked PEGDA samples of different molecular weights (20% w/v in water) at different light intensities between 20-100 % using a custom-built DLP platform (λ= 385nm, I= 5.2W/cm^2, working distance= 212 mm). **Average Resolution values for five light intensities are used to draw Figure 5-e.**

	Molecular weights (Da)			
Light Intensity	575	700	4000	6000
20%	196.2	187.3	315.1	396.1
40%	211.3	244.2	321.4	398.6
60%	222.7	245.5	306.3	359.4
80%	225.3	245.5	330.3	348.0
100%	220.2	250.6	307.5	318.9
Average Resolution [um]	215.1	234.6	316.1	364.2